

Research Articles | Behavioral/Cognitive

Acceleration and Velocity Dissociate Temporal Phases of Postural Control in Rhesus Macaques

<https://doi.org/10.1523/JNEUROSCI.0121-26.2026>

Received: 21 January 2026

Revised: 12 March 2026

Accepted: 20 March 2026

Copyright © 2026 the authors

This Early Release article has been peer reviewed and accepted, but has not been through the composition and copyediting processes. The final version may differ slightly in style or formatting and will contain links to any extended data.

Alerts: Sign up at www.jneurosci.org/alerts to receive customized email alerts when the fully formatted version of this article is published.

1 **Acceleration and Velocity Dissociate Temporal Phases of Postural Control in Rhesus**
2 **Macaques**

3 Running title: Acceleration- and Velocity-Dependent Postural Phases

4 Olivia M.E. Leavitt Brown¹, Bassil A. Ramadan¹, Kathleen E. Cullen^{1,2*}

5

6 ¹Department of Biomedical Engineering, Johns Hopkins University, Baltimore, MD, 21205

7 ²Department of Neuroscience, Department of Otolaryngology-Head and Neck Surgery, Kavli
8 Neuroscience Discovery Institute, Johns Hopkins University, Baltimore, MD, 21205

9 *Corresponding author (email: kathleen.cullen@jhu.edu)

10 **Abstract**

11 Maintaining balance requires the nervous system to transform sensory signals about
12 unexpected postural perturbations into precisely timed motor commands. Although human
13 studies have established that postural responses unfold in distinct temporal phases, how
14 specific kinematic variables structure these phases during rotational perturbations remains
15 unresolved, because angular acceleration and velocity are typically confounded. Here, we
16 developed a rhesus macaque model of postural control that independently manipulates angular
17 acceleration and peak velocity during transient pitch and roll tilts in monkeys of either sex. By
18 simultaneously measuring head kinematics—directly relevant to vestibular signaling—and
19 center-of-pressure dynamics, we quantified how sensory inputs and motor outputs evolve
20 across successive phases of the postural response. We show that short-latency postural
21 responses (<100 ms) are primarily governed by angular acceleration, whereas medium-latency
22 responses (100–200 ms) scale with angular velocity. This dissociation was robust across
23 perturbation axes and accompanied by axis-dependent control strategies: roll tilts elicited
24 constrained head motion consistent with active stabilization in space, whereas pitch tilts
25 produced more compliant, platform-following behavior. Together, these findings identify distinct
26 kinematic variables governing successive phases of balance control and establish a primate
27 framework for linking neural circuit activity to the temporal organization of postural responses.

28

29 **Significance Statement**

30 Maintaining balance requires transforming sensory signals about unexpected body motion into
31 precisely timed motor commands. Progress in understanding this process has been limited
32 because angular acceleration and velocity are inherently coupled during rotational
33 perturbations. Here, using a rhesus macaque model, we dissociate these kinematic variables
34 and show that they govern distinct temporal phases of postural control: angular acceleration
35 determines short-latency (<100 ms) responses, whereas angular velocity shapes medium-
36 latency (100–200 ms) adjustments. We further demonstrate axis-dependent postural strategies
37 that parallel those observed in humans. Together, these findings resolve a longstanding
38 confound in balance research and establish a primate framework that will enable future studies
39 to link neural circuit activity to the biomechanics of postural control.

40 Introduction

41 Maintaining stable posture in a dynamic environment is essential for everyday activities, and
42 failures of postural stability are a leading cause of falls and mobility impairments (Kakara et al.,
43 2024; Moreland et al., 2023). Stability depends on the integration of vestibular, visual, and
44 proprioceptive inputs to generate coordinated reflexive and voluntary motor responses (Forbes
45 et al., 2020; Mergner et al., 2009). From a neural systems perspective, this requires
46 transforming multisensory information about unexpected perturbations to the body into motor
47 commands that are precisely timed across distinct temporal phases. However, how specific
48 kinematic variables shape these phases during rotational perturbations remains unresolved. We
49 therefore tested whether angular acceleration and velocity selectively govern early and later
50 phases of rotational postural responses.

51 Human studies of translational perturbations have established a temporal organization of
52 postural responses, with short-latency components dominated by somatosensory inputs and
53 medium-latency components shaped by vestibular signals (Allum et al., 2003; Diener et al.,
54 1988; Forbes et al., 2020; Horak et al., 1990; Inglis & Macpherson, 1995). In these paradigms,
55 acceleration and velocity were historically confounded, but later work demonstrated that
56 acceleration primarily governs short-latency responses, whereas velocity shapes medium-
57 latency adjustments (Welch & Ting, 2009). Whether a similar dissociation governs postural
58 control during rotational perturbations—where semicircular canal signals are central—remains
59 unknown.

60 Rotational perturbations provide a sensitive assay for probing vestibular contributions to
61 balance, as responses are disproportionately impaired following vestibular loss (cat: Inglis &
62 Macpherson, 1995; human: Horak et al., 2016). Prior studies have further revealed axis-
63 dependent strategies: roll tilts typically elicit symmetric stabilizing responses, whereas pitch tilts
64 often produce forward–backward asymmetries and greater platform-following motion (Allum et
65 al., 2008; Carpenter et al., 2001; Horak et al., 2016; Mansfield & Maki, 2009; Welch & Ting,
66 2009). However, in all prior rotational studies, angular acceleration and velocity have remained
67 inherently coupled, preventing independent assessment of their contributions to successive
68 temporal phases of the postural response.

69 Accordingly, here we developed a rhesus macaque model of postural control that independently
70 manipulates angular acceleration and peak velocity during transient pitch and roll tilts. Rhesus
71 macaques share key biomechanical features with humans, including plantigrade stance and
72 comparable base-of-support geometry, while permitting direct recordings from and
73 manipulations of neural circuits that are not feasible in human subjects. At the same time,
74 interspecies differences, including variations in center-of-mass height relative to limb length,
75 habitual postural configuration, and base-of-support geometry, preclude direct extrapolation
76 from human data and necessitate species-specific behavioral benchmarks to enable meaningful
77 interpretation of future neurophysiological findings. Providing benchmarks for rhesus monkey
78 postural control within this framework enables future neurophysiological investigations—
79 combining single-neuron recordings and causal circuit manipulations—that can directly link
80 neural circuit activity to postural control. By disentangling acceleration and velocity, we directly
81 test how the nervous system parses unexpected postural perturbations into temporally distinct
82 control signals. Because head motion both drives vestibular afferent activity and reflects
83 postural motor output within a closed-loop system, we simultaneously quantified six-dimensional
84 head kinematics together with center-of-pressure dynamics. Our findings show that short-

85 latency postural responses (0-100 ms) are primarily governed by angular acceleration, whereas
86 medium-latency responses (100–200 ms) scale with angular velocity. This dissociation extends
87 principles previously established for translational perturbations to rotational postural control. In
88 addition, roll tilts elicited constrained head motion consistent with enhanced stabilizing control in
89 space, whereas pitch tilts produced more compliant, platform-following behavior, revealing axis-
90 dependent postural strategies. Together, our findings identify distinct kinematic variables that
91 structure successive phases of balance control and establish a primate framework for linking
92 neural circuit activity to the temporal organization and control variables of postural responses.

93 **Methods**

94 Three rhesus monkeys (*Macaca mulatta*; two male, 'Monkey E' and 'Monkey B,' and one
95 female, 'Monkey D') were used in this study. Each animal completed ≥ 20 trials per perturbation
96 condition across multiple stimulus conditions. All experimental procedures were approved by the
97 Johns Hopkins Animal Care and Use Committee (ACUC, protocol number PR22M342). The
98 ACUC is accredited by the American Association for the Accreditation of Laboratory Animal
99 Care (AAALAC) and is in compliance with the guidelines of the Office of Laboratory Animal
100 Welfare at the National Institutes of Health. As described previously (Zobeiri & Cullen, 2022),
101 each animal was anesthetized and equipped with a titanium post fastened to the skull using
102 titanium screws and dental acrylic to allow immobilization of the head and securing of recording
103 hardware. All animals recovered for at least two weeks before experiments began.

104 *Experimental Setup*

105 The experimental setup consisted of a hexapod motion platform (SYMETRIE, Nimes, France)
106 onto which was mounted a custom-built, clear-sided behavioral chamber with a fiberglass
107 frame. The behavioral chamber is a total of 2.5m in length to accommodate walking
108 experiments, but Plexiglas dividers allow for confinement of the animal to any of three sections.
109 The chamber was 0.5m wide and 0.75 m high, allowing animals of any size to sit, stand, walk
110 several strides, and turn around. All experiments reported here took place with the animal
111 confined to the central section of the chamber, which was 0.7 m long and was also instrumented
112 with a force plate. The custom-built force plate consisted of four ABS plastic footplates each
113 mounted to a uniaxial load cell (Omega Engineering, Sunbury, OH), all of which were mounted
114 to a single baseplate. Animals were transported from the colony room to the setup in a standard
115 primate chair, then fitted with a wireless, wearable inertial measurement unit (IMU; Shimmer
116 Sensing, Dublin, Ireland) and 3D-printed optical orientation tracker (Vagvolgyi et al., 2022)
117 affixed to their head fixation post. Additionally, four high-speed cameras (Teledyne FLIR,
118 Wilsonville, OR) were mounted around the setup to capture video of the animals, which was
119 used post hoc to confirm that postural responses were free of step responses.

120 *Perturbation Design*

121 Perturbations were explicitly designed to dissociate angular acceleration from peak velocity
122 while maintaining comparable total displacement. Perturbations were designed in MATLAB by
123 first constructing an angular acceleration time series which included an acceleration and
124 deceleration block with the desired peak acceleration amplitude, and duration and inter-block
125 interval that together yielded the desired peak velocity and total displacement. The acceleration
126 blocks were constructed to mimic, as closely as possible, a step change in acceleration given
127 the temporal resolution of the hexapod motion platform (100 samples/sec). This acceleration

128 signal was then double-integrated, and the resulting position signal was fed into the motion
129 platform.

130 Perturbations were based on those used in similar previous experiments in humans (Allum et
131 al., 2008; Carpenter et al., 2001) and cats (Inglis & Macpherson, 1995), which had a peak
132 velocity of 40 deg/s and an estimated angular acceleration of 500 deg/s². These values were
133 used as the standard “base” perturbation, which was shared between the set varying angular
134 acceleration, and the set varying peak velocity. For each set (velocity and acceleration) a higher
135 and lower value than the base perturbation was used: 200 and 1000 deg/s² accelerations, and
136 20 and 60 deg/s peak velocities. This yielded a total of five perturbations, which were delivered
137 in four directions: forward and backward pitch, and leftward and rightward roll. Overall, there
138 were 20 perturbation conditions.

139 *Conceptual Biomechanical Model.*

140 To provide mechanistic intuition for how passive mechanical properties can shape head and
141 body motion during platform tilts, we implemented a conceptual, simplified dual-pendulum
142 biomechanical model. The model represents the body as two rigid segments: a trunk–limb
143 segment pivoting about the ankles and a head segment articulated at the neck.

144 Platform perturbations were imposed by prescribing the angular velocity of the support surface
145 as a time-varying input, mirroring the experimental perturbation design. This velocity signal was
146 numerically integrated to obtain platform angular displacement. The equations of motion
147 included linear stiffness and damping terms coupling the trunk to the rotating platform, as well
148 as stiffness and damping terms coupling the head to the trunk (see Supplementary Table S1).

149 Segment masses, lengths, and moments of inertia were set to representative values based on
150 standard rhesus monkey biometric tables (Vilensky, 1979). Because neck and body stiffness
151 have not been directly measured in monkeys, stiffness and damping parameters were chosen
152 within physiologically plausible ranges reported for cats and humans (Goldberg & Peterson,
153 1986; Keshner et al., 1992; Peng et al., 1996; Ting & Macpherson, 2004). Importantly, these
154 parameters were not tuned to fit the experimental data but were selected solely to illustrate
155 qualitatively distinct regimes of platform-following versus head-in-space stabilization, rather than
156 to reproduce the experimental responses.

157 Torques on the trunk and head were computed using the following equations, where θ_1 and θ_2
158 denote trunk and head angles relative to vertical, respectively, φ denotes platform angle, and
159 overdots indicate time derivatives:

160 Torque on trunk (τ_1):

$$161 \tau_1 = -m_1 \cdot g \cdot l_1 \cdot \theta_1 - k_{platform} \cdot (\theta_1 - \varphi) - c_{platform} \cdot (\dot{\theta}_1 - \dot{\varphi})$$

162 Torque on head (τ_2):

$$163 \tau_2 = -k_{neck} \cdot (\theta_2 - \theta_1) - c_{neck} \cdot (\dot{\theta}_2 - \dot{\theta}_1)$$

164 Here, m_1 , l_1 , and I_1 denote trunk mass, center-of-mass distance, and moment of inertia,
165 respectively; I_2 denotes head moment of inertia; and k and c terms represent stiffness and
166 damping coefficients.

167 Angular accelerations were computed as:

168 $\theta_1 = \tau_1/I_1$

169 $\theta_2 = \tau_2/I_2$

170 Head and trunk angles and angular velocities were obtained by numerically integrating the
171 resulting system of ordinary differential equations using MATLAB's ODE45 solver.

172

173 *Behavioral Training & Measurement*

174 As stated in the description of the behavioral setup, the behavioral chamber was instrumented
175 with a force plate, and the animal wore a wireless IMU and an optical tracker secured to its
176 headpost during training and experimental sessions. Each monkey was acclimated to the
177 behavioral chamber over the course of three training sessions, which took approximately one
178 week. During the first session, the monkey was repeatedly transferred between the transport
179 chair and the behavioral chamber and rewarded with food treats following each transfer attempt.
180 During the second session, the animal was allowed to enter the central chamber and freely
181 explore the space with intermittent juice rewards from a spout fixed to the ceiling of the
182 chamber; animals quickly learned to orient themselves toward the reward spout. During the third
183 session, the animal was again transferred to the chamber, and sinusoidal platform motions were
184 applied to acclimate the animal to platform movement, minimizing startle responses during
185 experiments. Each of these behavioral training sessions took between 30 minutes and 2 hours.
186 The longest training session exceeded the duration of most experimental sessions, ensuring
187 acclimation to extended periods in the setup.

188 Experimental sessions began after the animal had completed training sessions and reinforced
189 the trained standing behavior throughout testing. For each experimental session, the animal
190 was first transferred to the chamber and stood on the force plate. Data from the force plate were
191 continuously fed to a real-time experimental control computer, and the force distribution across
192 each of the four panels was calculated. Head orientation data from the optical head tracker were
193 fed into the same system. To ensure consistent initial stance, the animal was required to stand
194 symmetrically at trial onset. The criteria for starting a trial included having one paw on each
195 footplate with weight balanced across the four footplates (i.e., <10 N difference between the
196 front and back halves and between the left and right halves of the force plate). The animal also
197 needed to have its head vertical and facing straight ahead (deviations <10° in any axis).
198 Transient trials began at random times, occurred in a randomized order, and shared identical
199 total displacement to minimize anticipatory postural responses. Before each trial, the
200 experimenter initiated recording on the motion capture cameras, while the force plate and IMU
201 recorded continuously at 1,000 samples/s. Data collection sessions lasted as long as the animal
202 remained cooperative with the experiment. For each monkey, a minimum of 20 trials were
203 collected per condition.

204

205 *Data Analyses*

206 Following experiments, data were calibrated and synchronized in MATLAB using a custom code
207 pipeline. Data from the load cells under each footplate of the force plate were converted to
208 center of pressure (CoP) position according to the following equations:

209
$$CoP_{Lat} = \frac{(F_{FL} + F_{HL}) - (F_{FR} + F_{HR})}{m}$$

210
$$CoP_{AP} = \frac{(F_{FL} + F_{FR}) - (F_{HL} + F_{HR})}{m}$$

211 where F_{FL} , F_{FR} , F_{HL} , and F_{HR} represent the forces on the front left, front right, hind left, and hind
212 right plates, respectively, and m represents the mass of the monkey. Data from the IMUs were
213 calibrated onboard and synchronized to the same clock onboard each device.

214 Camera data were fed through DeepLabCut and Anipose (Karashchuk et al., 2021; Mathis et
215 al., 2018) for markerless pose reconstruction. This video-based data was primarily used to
216 determine whether step responses occurred during a trial; trials containing step responses were
217 excluded from further analysis. Trials were also removed by the program if head velocity in the
218 500 ms preceding a trial exceeded 20 deg/s, and if head velocity at any point in the trial
219 (including 500 ms before the onset and after the offset of motion) exceeded 400 deg/s, which
220 indicated head shaking or other voluntary movement contaminating the animal's postural
221 response. Approximately 10% of trials collected for each monkey were excluded based on
222 video, kinematic, or kinetic data. This rate of exclusion was comparable between animals.

223 Trials of the same perturbation in the same animal were then synchronized, and the mean
224 response and standard error were computed. We then computed the mean response across the
225 first 100 ms following perturbation onset (short-latency window) and during the 100–200 ms
226 interval (medium-latency window). Response onset latency was defined as the first time point at
227 which the response exceeded the root mean square (RMS) error computed over the 500 ms
228 preceding perturbation onset. Total angular displacement was computed as the integral of
229 angular velocity, total linear displacement as the double integral of acceleration, and CoP
230 trajectory length as the cumulative sum of the CoP response (Lemay et al., 2014). All
231 displacement measures were computed over the entire duration of the platform motion.

232 Finally, to quantify symmetry between responses to perturbations in opposite directions (left vs.
233 right, forward vs. backward), we computed an “asymmetry index” (adapted from Kong et al.,
234 2010). For the within-direction comparison, we calculated the distribution of the mean absolute
235 percentage error (MAPE) across all possible pairs of responses to the same stimulus within a
236 given direction (e.g., all leftward responses, all rightward responses). The resulting distributions
237 for the two opposing directions were then combined to yield the first distribution. For the across-
238 direction comparison, we inverted the responses for one direction and then calculated the
239 MAPE across all possible pairs of responses regardless of direction, producing a second
240 distribution. The asymmetry index was defined as the difference between the mean values of
241 these two distributions.

242 *Statistical Analyses*

243 Statistically significant differences between monkeys and between conditions within the velocity
244 and acceleration sets were established using a two-way ANOVA accounting for unequal sample
245 sizes. A significance threshold of $p < 0.025$ was used for differences between monkeys and
246 differences between conditions to control for multiple comparisons across factors. When a
247 significant main effect was detected in the ANOVA, linear regression was used to quantify the
248 dependence of the pooled responses across all monkeys on angular acceleration or peak
249 velocity, as appropriate. Significance of the asymmetry index was assessed using a two-tailed t-

250 test ($\alpha = 0.05$), with the null hypothesis of symmetry (no difference between distributions) and
251 the alternative hypothesis of asymmetry. For each perturbation axis, p-values across monkeys
252 and stimuli were then combined using Fisher's method.

JNeurosci Accepted Manuscript

253 Results

254 In this study, we examined the postural responses of rhesus monkeys to tilt perturbations on a
255 hexapod motion platform (**Fig. 1A**). Our goal was to establish a nonhuman primate model of
256 postural control and determine how different kinematic variables—axis, angular velocity, and
257 acceleration—influence postural strategies. Three monkeys were trained to stand symmetrically
258 in a natural perching posture on a force plate, with their heads level and facing forward. Each
259 animal was outfitted with a head-mounted inertial measurement unit (IMU) and an optical
260 tracking marker (Vagvolgyi et al., 2022) to ensure initial head alignment was consistent across
261 trials. Once trained, we applied tilt perturbations and recorded the resulting head motion and
262 center-of-pressure (CoP) responses. Tilt perturbations were applied in both pitch
263 (forward/backward) and roll (left/right) axes (**Fig. 1B**), with peak velocity and angular
264 acceleration varied independently to isolate their specific contributions (**Fig. 1C**). High-speed
265 video from four cameras was analyzed using 3D markerless pose estimation (i.e., DeepLabCut
266 and Anipose, (Karashchuk et al., 2021; Mathis et al., 2018)) to confirm the absence of stepping
267 or non-postural voluntary movements such as head shaking. **Figure 1D** illustrates a simple
268 dual-pendulum model used here as a conceptual framework to distinguish passive mechanical
269 responses from active stabilization. Varying body–platform coupling and neck stiffness produces
270 qualitatively distinct head and body kinematics, providing intuition for how different postural
271 strategies—ranging from platform-following to stabilization in space—can arise even in the
272 absence of active neural control.

273 Modulation of Pitch Postural Responses by Stimulus Velocity

274 Most prior studies of postural control have focused on rotational perturbations in the pitch axis
275 (reviewed in Forbes et al., 2020). Thus, we began by examining responses to pitch tilts to
276 specifically address how postural responses vary as a function of peak velocity. Importantly, by
277 holding angular acceleration constant, we were able to isolate velocity-specific effects. We first
278 applied transient forward pitch tilts (of 20, 40, or 60 deg/s) with a fixed angular acceleration (500
279 deg/s²) - parameter values based on prior work in quadrupedal cats (Macpherson et al., 2007;
280 **Fig. 1B**). Mean head velocity, acceleration, and CoP (center of pressure) along the perturbation
281 axis are shown for each monkey in **Figure 2A** (Monkey D) and **Figure S1A, B** (Monkey E &
282 Monkey B).

283 Overall, we found that pitch perturbations reliably elicited head movements in monkeys that
284 closely resembled those previously reported in cats (Macpherson et al., 2007; Torres-Oviedo et
285 al., 2006). These head motion responses were relatively consistent across animals and showed
286 low trial-to-trial variability, particularly 100 ms after the onset of the perturbation. To quantify
287 their temporal dynamics, we defined two windows of interest based on the prior literature: a
288 short-latency window (0–100 ms) and a medium-latency window (100–200 ms) (**Fig. 2A** yellow
289 and green shaded regions, respectively; Allum et al., 2003; Diener et al., 1988; Forbes et al.,
290 2020; Horak et al., 1990; Inglis & Macpherson, 1995). Within each window, we then computed
291 the mean head pitch velocity, fore-aft acceleration, and CoP response. **Figures. 2B-D** plot the
292 results of this analysis, for short-latency (yellow), medium-latency (green), onset latency (white,
293 left), and distance traversed (white, right) measurements for each of the three transient
294 perturbation profiles (i.e., peak velocities reaching 20, 40, or 60 deg/s). The results for each
295 individual monkey are provided in **Fig. S1C-E**.

296 *Head motion responses:* Our analysis of head pitch velocity revealed that, in the short-latency
297 window (**Fig. 2B**, yellow panel), mean head pitch velocity remained relatively constant across
298 velocities. In contrast, during the medium-latency window (**Fig. 2B**, green background), pitch
299 velocity increased systematically with stimulus velocity, demonstrating significant velocity-
300 dependent modulation. Correspondingly, our analysis of fore-aft translational head acceleration
301 revealed a similar pattern (**Fig. 2C**); medium-latency responses decreased significantly,
302 increasing in magnitude as a function of stimulus velocity (**Fig. 2C**, green background), whereas
303 this was not the case for short-latency acceleration responses (**Fig. 2C**, yellow panel). Onset
304 latencies of head pitch velocity and fore-aft translational acceleration were comparable (largely
305 within 50ms) and did not differ significantly across velocity conditions (**Fig. 2B,C** left white
306 panels), indicating that response onset was independent of peak stimulus velocity. Furthermore,
307 total head pitch displacement was 10 degrees in each case, indicating that the monkey rode on
308 the platform over the course of the perturbation (**Fig 2B**, right white panel). Unless otherwise
309 noted, onset latencies and total displacements of head and CoP motion were invariant across
310 conditions. Together, these results indicate that rhesus monkey head motion responses to pitch
311 tilts exhibit significant velocity-dependent modulation, which emerges primarily during the
312 medium-latency phase.

313 *CoP measures:* We next assessed fore-aft CoP displacement as a dynamic indicator of whole-
314 body stabilization to pitch perturbations (**Fig. 2D**). In contrast to head motion kinematics, CoP
315 responses demonstrated significant velocity dependence during the short-latency window (**Fig.**
316 **2D**, left panel) as well as the medium-latency window (**Fig. 2D**, green panel), with both
317 increasing significantly as a function of velocity. Qualitative inspection of the CoP traces in Fig
318 2A further revealed that the peak CoP response was coincident with the peak velocity of the
319 platform perturbation. This time point occurred within the short-latency window during the 20
320 deg/s condition and the medium-latency window during the 40 and 60 deg/s conditions,
321 suggesting that velocity-scaled adjustments may occur coincident with this transition point.
322 Taken together, these results demonstrate that pitch perturbations generally elicited a passive
323 “ride-the-platform” response (Buchanan & Horak, 2001) – where the animal’s head and body
324 moved along with the platform rather than stabilized relative to space, with velocity modulating
325 medium-latency adjustments. Within the conceptual framework illustrated in **Fig. 1D**, this pattern
326 qualitatively resembles a regime in which the body is strongly coupled to the platform while the
327 neck remains compliant, resulting in platform-following motion of the trunk and lagged head
328 motion.

329 *Direction-Dependent Modulation:* We next quantified responses to backward tilts. **Figure 3**
330 shows the same analyses applied to forward tilts (**Figure 2**) but for backward tilts with the same
331 fixed angular acceleration (500 deg/s^2) and peak velocities of 20, 40, or 60 deg/s. In contrast to
332 forward tilts, responses to backward perturbations were less stereotyped across animals
333 (compare **Fig. 3A** and **Fig. S2A,B**). Correspondingly, there were significant differences in mean
334 velocity between monkeys during both the short and medium-latency window (**Fig. S2C**). On
335 average, pitch velocity in the short-latency window remained unchanged across stimulus
336 velocities (**Fig. 3B**, yellow panel), whereas it significantly increased in magnitude as a function
337 of stimulus velocity (i.e., continued to move along with platform as speed increased) in the
338 medium-latency window (**Fig. 3B**, green panel). Interestingly, at the lowest peak velocity head
339 pitch displacement was around 10 degrees, demonstrating a riding-the-platform response. Total
340 displacement also decreased significantly with increasing velocity, indicating greater
341 compensation as velocity increased (**Fig. 3B**, right white panel). Head acceleration responses

342 also followed this pattern: Mean acceleration in the short-latency window did not vary with
343 stimulus velocity (**Fig. 3C**, yellow panel), but increased significantly in the medium-latency
344 window (**Fig. 3C**, green panel).

345 Lastly, while head movement responses were less stereotyped across monkeys for backward
346 versus forward pitch perturbations, quantification of CoP revealed similarities across monkeys
347 (**Fig. 3D**, **Fig. S2E**). As for forward tilts, CoP responses to backward tilts exhibited significant
348 velocity-related effects during both the short- and middle-latency windows (**Fig. 3D**, yellow and
349 green panels), increasing in magnitude as a function of increasing velocity. Thus, like forward
350 tilts, CoP responses to backward tilts were modulated by stimulus velocity even during the
351 short-latency phase. Further, similar to forward tilts, these results indicate that backward tilt
352 perturbations generally elicit a passive “ride-the-platform” response at low velocity, with
353 increasing compensation at higher velocities.

354 **Modulation of Roll Postural Responses by Stimulus Velocity**

355 We next applied tilt perturbations in the roll axis, again varying peak velocity independently of
356 acceleration (**Figure 4**). In contrast to the markedly asymmetrical response to forward versus
357 backward pitch tilts described above, responses to leftward and rightward roll tilts were relatively
358 symmetrical across animals (compare **Fig. S3 A** versus **B**). We quantified this observation by
359 computing an asymmetry index for leftward versus rightward, and forward versus backward tilt
360 perturbations (see Methods). Overall, we found that roll responses were consistently
361 symmetrical across monkeys, while pitch responses were a mix of symmetrical and
362 asymmetrical. Given that roll perturbation response were relatively symmetric, we inverted
363 responses to rightward perturbations and combined them with those from leftward perturbations
364 in our analysis, resulting in a total of 40 trials per condition.

365 Notably, unlike pitch perturbations, roll tilts revealed a qualitatively distinct postural strategy,
366 characterized by constrained head motion suggestive of active stabilization. Overall, individual
367 monkeys generated more consistent responses to roll than pitch perturbations (e.g., compare
368 **Fig. 4A** versus **Fig. 2A & Fig. 3A**). Moreover, whereas monkeys tended to ride the platform
369 during pitch tilts, head motion during roll perturbations appeared to be actively constrained—not
370 exceeding the maximum platform velocity of 60 deg/s, and in the case of Monkey D, never
371 exceeding the peak platform velocity of the condition. This result suggests a fundamentally
372 different postural strategy in the roll axis, emphasizing active stabilization over passive
373 compliance. Within the conceptual framework illustrated in Fig. 1D, this behavior falls outside
374 the range expected from passive body–platform mechanics and instead corresponds to a
375 regime requiring active stabilization to constrain head motion relative to space.

376 To next quantify how stimulus velocity shaped this active stabilization strategy, we measured
377 head roll and lateral head movement and CoP responses in short and medium-latency windows
378 (**Fig 4B-D**, individual monkey responses in **Fig. S4**). We then compared these measures across
379 the three perturbation conditions (i.e., 20, 40, or 60 deg/s).

380 *Head motion:* During the short-latency window, mean head roll velocity did not vary linearly as a
381 function of velocity (**Fig. 4B**, yellow). Medium-latency responses, however, showed inter-subject
382 variability, with two monkeys demonstrating oppositely directed trends, and the third monkey
383 showing no velocity-dependent scaling (**Fig. S4**, green). This heterogeneity resulted in no
384 overall effect of acceleration on medium-latency responses (**Fig. 4B**, green). Similarly, mean
385 lateral head acceleration during the short-latency window was unaffected by peak velocity (**Fig.**

386 **4C**, yellow). However, as observed for pitch perturbations, mean head acceleration increased
387 significantly with stimulus velocity during the medium-latency window (**Fig. 4C**, middle). Finally,
388 total roll displacement was consistent across velocities and fell within the band between perfect
389 compensation and perfect riding (i.e., between 0 and 10 degrees) for all monkeys, indicating
390 partial compensation for the platform motion (**Fig 4B**, right white).

391 *CoP measures*: Both short-latency (**Fig. 4D**, yellow) and medium-latency CoP responses (**Fig.**
392 **4D**, green) increased significantly with peak velocity, thereby paralleling the trends observed
393 above for backward and forward pitch.

394 Thus, in summary, rhesus monkeys showed axis-dependent postural strategies to transient tilt
395 perturbations. For pitch tilts in both the forward and backward directions, monkeys tended to
396 “ride” the platform, showing minimal compensation, and head motion responses were velocity-
397 dependent in the medium-latency window, while CoP responses showed velocity-dependent
398 effects in both short- and medium-latency phases. In contrast, the smaller head-in-space motion
399 responses to roll tilts indicated active compensation for platform motion, and were less velocity
400 dependent. However, CoP measures again scaled with velocity in both latency windows, which
401 suggests that the active compensation at the support surface which ultimately constrains head
402 motion is modulated by velocity.

403 **Modulation of Pitch and Roll Postural Responses by Stimulus Acceleration**

404 So far, we have shown that peak velocity predominantly modulates responses in the medium-
405 latency window. We next hypothesized that acceleration—when varied independently—would
406 also shape short-latency responses based on prior studies of translational perturbations (Welch
407 & Ting, 2009). To test this proposal, we applied tilt perturbations at three acceleration levels
408 (200, 500, and 1000 deg/s²) while holding peak velocity constant at 40 deg/s (**Fig. 1C**). Notably,
409 this design included a shared condition (500 deg/s² at 40 deg/s) with the experiments described
410 above focused on isolating the effect of velocity (**Fig. 1B**), enabling a direct comparison.

411 *Forward pitch*: We first examined head responses to acceleration-controlled forward pitch
412 perturbations (**Fig. 5A**). While in two monkeys there was a trend of increasing mean head pitch
413 velocity in the short-latency window (**Fig. S5**, monkeys E and B), overall, quantification of
414 responses revealed that mean head pitch velocity showed significant differences between
415 accelerations but without a linear dependence (**Fig. 5B**, left panel). Likewise, quantification of
416 responses in the medium-latency window mean head velocity increased as a function of
417 acceleration across animals (**Fig. 5B**, middle). In contrast, head fore-aft linear acceleration was
418 not significantly influenced by acceleration in either the short-latency (**Fig. 5C**, left), or medium-
419 latency (**Fig. 5C**, middle) windows.

420 Overall, quantification of CoP responses revealed the most striking acceleration-dependent
421 effects. Mean CoP response in the short-latency window increased significantly with
422 acceleration (**Fig. 5D**, yellow) while the response in the medium-latency window remained
423 unchanged (**Fig. 5D**, green). Furthermore, onset latency shifted significantly earlier with
424 increasing acceleration (**Fig. 5D**, white, left), providing compelling evidence for acceleration-
425 specific control of early postural responses. The distance traversed by the CoP was again small,
426 indicating that the animals typically rode on the platform in pitch (**Fig 5D**, white, right).

427 *Backward pitch*: We next examined responses to acceleration-controlled backward pitch
428 perturbations (**Fig. 6A**). Two monkeys showed clear linear increases in pitch velocity during the

429 medium-latency window, while a third monkey exhibited a similar increase in the short-latency
430 window (**Fig. S6C**, left and middle panel). Despite these individual trends, however, overall
431 head pitch velocity did not vary systematically with acceleration in either the short- (**Fig. 6B**,
432 **yellow**) or medium-latency windows (**Fig. 6B**, green). In contrast, head fore-aft linear
433 acceleration was systematically modulated across both windows: short-latency responses
434 increased significantly with acceleration (**Fig. 6C**, yellow), whereas medium-latency responses
435 decreased significantly (**Fig. 6C**, green). Additionally, the latency of the head pitch response,
436 but not fore-aft translation, became significantly earlier with increasing acceleration (**Fig. 6B**,
437 white, left), while acceleration onset timing remained unchanged (**Fig. 6C**, white, left). Notably,
438 as with backward pitch of increasing velocity, backward pitch displacement fell more in the
439 compensating window than for forward pitch and was significantly different between
440 accelerations, but without a linear trend (**Fig. 6B**, white, right).

441 Finally, CoP responses scaled robustly with acceleration in the short-latency window (**Fig. 6D**,
442 yellow) but remained unchanged in the medium-latency window (**Fig. 6D**, green). The onset of
443 the CoP response also occurred significantly earlier with higher accelerations (**Fig. 6D**, white,
444 left). Interestingly, short-latency CoP responses in the high-acceleration condition were smaller
445 than those in other axes and CoP total distance traversed was smaller (**Fig 6D**, white, right),
446 likely reflecting biomechanical constraints of the monkeys' posture—forelimbs extended and
447 hindlimbs flexed—which may limit rapid compensatory responses to backward perturbations, as
448 well as animal-specific strategies.

449 *Roll axis:* Using our constant-velocity protocol, we likewise recorded postural responses to roll
450 tilts (Monkey D: **Fig. 7A**, Monkey E: **Fig. S7A**, Monkey B: **Fig. S7B**). Consistent with pitch
451 perturbations, early head motion in roll showed acceleration-dependent modulation. Although
452 roll velocity in the short-latency window was unaffected by acceleration (**Fig. 7B**, yellow), the
453 onset of the roll velocity response occurred significantly earlier with increasing acceleration (**Fig.**
454 **7B**, white, left). Notably, head roll displacement was unaffected by platform acceleration and fell
455 in the partial compensation region (**Fig 7B**, white, right). Head lateral acceleration increased
456 significantly in the short-latency window (**Fig. 7C**, yellow), but showed no effect of acceleration
457 in the medium-latency window (**Fig. 7C**, green). In contrast, the onset latency of lateral
458 acceleration remained unchanged across conditions (**Fig. 7C**, white, left). Most strikingly, CoP
459 responses exhibited robust acceleration effects: short-latency CoP responses increased
460 markedly with higher accelerations (**Fig. 7D**, yellow), whereas medium-latency responses
461 remained unchanged (**Fig. 7D**, green). Additionally, CoP response onset occurred significantly
462 earlier as acceleration increased (**Fig. 7D**, white, left). Notably, this pattern contrasted with pitch
463 perturbations, where medium-latency CoP responses decreased with increasing acceleration,
464 highlighting axis-specific strategies—passive 'riding' in pitch versus active compensation in roll.

465 Taken together, these findings demonstrate that angular acceleration modulates the short-
466 latency postural response in head velocity, acceleration, and center-of-pressure dynamics—
467 without significantly altering the magnitude of the medium-latency response—reinforcing the
468 idea that acceleration shapes the dynamics, but not the magnitude, of early motor responses.
469 More broadly, our results show that rhesus monkey postural responses closely mirror those of
470 humans, supporting their use as a translational model for studying balance control. Most
471 notably, we identify a clear dissociation between the contributions of acceleration and velocity:
472 early (short-latency) responses are primarily driven by platform acceleration, while later
473 (medium-latency) responses are shaped by peak velocity. In the initial phase, limb forces

474 generated by acceleration dominate the compensatory response, whereas in the later phase,
475 adjustments reflect steady-state motion. This dissociation provides a foundational insight into
476 the sensory-motor basis of balance and offers a robust framework for future investigations into
477 postural control.

JNeurosci Accepted Manuscript

478 Discussion

479 By experimentally separating angular acceleration from velocity, we show that acceleration
480 primarily influences the earliest (short-latency) responses, whereas velocity modulates medium-
481 latency adjustments. The axis of rotation further shaped postural control strategies: roll tilts
482 evoked active stabilization of the body in space, whereas pitch tilts generally elicited a compliant
483 “ride-the-platform” response—moving along with the platform rather than stabilizing relative to
484 space (**Fig. 8**). By separating these kinematic variables, our results resolve a key limitation of
485 prior work and establish a primate framework that will enable future studies to directly link neural
486 circuit activity to the temporal organization of postural control.

487 *Axis-specific biomechanical strategies*

488 Extensive work in humans has characterized postural responses to rotational perturbations
489 about the roll and pitch axes (Allum et al., 2008; Carpenter et al., 2001; Goodworth et al., 2023;
490 Küng et al., 2009; Mansfield & Maki, 2009; Welch & Ting, 2009). In our nonhuman primate
491 model, roll responses were highly symmetrical for leftward versus rightward tilts, whereas pitch
492 responses were asymmetrical for forward versus backward tilts. This axis-dependent pattern
493 mirrors human findings and reflects the expected symmetry along anatomically symmetric axes
494 versus asymmetry along anatomically asymmetric axes (Allum et al., 2008; Carpenter et al.,
495 2001; Welch & Ting, 2009).

496 In the roll axis, head velocity remained substantially smaller in magnitude than platform motion,
497 indicating active stabilization of the body in space. This result is consistent with biomechanical
498 predictions: the allowable center-of-mass excursion before balance is threatened depends on
499 the ratio of base-of-support width to center-of-mass height in the axis of the perturbation
500 (Forbes et al., 2018). Because this ratio is similar in humans and macaques in roll (Fryar et al.,
501 2021; Vilensky, 1979), we predicted comparable postural strategies across species. Consistent
502 with this prediction, rhesus monkeys exhibited roll stabilization similar to that reported in
503 humans (Allum et al., 2008; Carpenter et al., 2001). Moreover, the only prior study examining
504 roll perturbations in monkeys—using continuous pseudorandom stimulation—also found
505 postural sway to be smaller than platform displacement (Thompson et al., 2016), supporting the
506 robustness of roll stabilization across perturbation paradigms.

507 In contrast, pitch tilts elicited a more compliant postural strategy in which animals largely moved
508 with the platform, tolerating larger center-of-mass displacements before generating corrective
509 torques. This behavior likely reflects the elongated anteroposterior base of support produced by
510 coordinated fore- and hindlimb stabilization, which mechanically increases tolerance to pitch
511 perturbations. Strikingly, even the most dynamic pitch perturbations tested here (1000 deg/s²)
512 failed to elicit strong stabilizing responses, paralleling findings in quadrupedal cats (Jacobs &
513 Macpherson, 1996; Macpherson et al., 2007). Humans, in contrast, exhibit strong pitch
514 stabilization at much lower accelerations (260 deg/s²) (Allum et al., 2008; Carpenter et al., 2001;
515 Horak et al., 2016), but adopt cat- and monkey-like pitch strategies when assuming a
516 quadrupedal stance (Dunbar et al., 1986; Macpherson et al., 2007). Together, these
517 comparisons highlight how body morphology and base-of-support geometry shape axis-specific
518 postural strategies while preserving common vestibular control principles across species.

519 *Balance responses to rotational platform perturbations: dissociating acceleration from velocity*

520 Prior studies using rotational platform perturbations have consistently confounded angular
521 acceleration and peak velocity, precluding clear attribution of their relative contributions
522 (reviewed in Forbes et al., 2020). By contrast, prior studies focused on postural responses to
523 translational platform perturbations have successfully dissociated the effects of acceleration
524 versus velocity. Specifically, acceleration has been shown to dominate short-latency responses
525 to translational perturbations, while velocity primarily influences medium-latency components
526 (Allum et al., 1994; Allum & Pfaltz, 1985; Bloem et al., 2002; Diener et al., 1988; Horak et al.,
527 1990; Inglis & Macpherson, 1995; Maki & Ostrovski, 1993; Welch & Ting, 2009). Our study
528 extends this dissociation to rotational perturbations, demonstrating that short-latency responses
529 are primarily acceleration-driven, whereas medium-latency responses scale with velocity.
530 Notably, this parallel across perturbation types emerges despite fundamental differences in
531 destabilizing mechanics—translation destabilizes posture through trunk inertia, whereas
532 rotational tilt can initially be mechanically stabilizing (Lippi et al., 2023; reviewed in Mergner et
533 al., 2009). Because each monkey contributed many repeated trials across conditions, the within-
534 subject design enabled robust quantification of response dynamics, and the dissociation
535 between acceleration-dependent short-latency responses and velocity-dependent medium-
536 latency responses was consistent across animals.

537 Overall, the present study establishes that, paralleling translational perturbations, stability during
538 dynamic tilts follows a systematic and dissociable temporal sequence. Such a sequence
539 requires continuous estimation and correction of body orientation relative to both the support
540 surface and gravity, implemented through precisely timed and scaled joint torques (Missen et
541 al., 2023; Peterka, 2018). By orthogonalizing angular acceleration and peak velocity, our design
542 provides the first clear demonstration of this dissociation in rotational postural control, offering a
543 methodological framework that can now be extended to probe the neural circuits that implement
544 these computations.

545 *Vestibular contributions revealed by head motion*

546 Most postural studies focus on CoP, limb kinematics, or EMG, yet head motion provides a direct
547 measure of the stimulus driving vestibular afferents and the resulting motor response. Because
548 vestibular afferents encode head motion itself (reviewed in Cullen 2019), voluntary head
549 movements simultaneously represent motor outputs and sensory signals for self-motion
550 encoding. Consequently, vestibular signals encoding head-centered motion must be
551 transformed into body-centered coordinates to generate appropriate postural adjustments
552 (Keshner & Dhaher, 2008; Mergner, 2007; Peterka, 2002). Because platform tilts move the
553 entire support surface, postural responses reflect integrated vestibular and somatosensory
554 feedback: head kinematics characterize the vestibular stimulus, whereas postural motion
555 reflects multisensory feedback integration. For this reason, we quantified head kinematics
556 together with CoP dynamics to capture both the vestibular stimulus and the resulting whole-
557 body postural response.

558 In the present study, direct measurements of six-dimensional head motion revealed that, like
559 CoP, evoked head motion was influenced by both acceleration and velocity. Notably, compared
560 to the few prior human studies that have measured head motion responses, head motion in
561 monkeys began substantially earlier—within ~60 ms for transient roll stimuli and as early as ~20
562 ms for pitch—versus ~80–120 ms in humans (Allum, 1992; Carpenter et al., 2001; Horak &
563 Macpherson, 1996). This difference in onset timing likely reflects a combination of
564 biomechanical and stimulus factors, including shorter limb lengths and our use of higher angular

565 accelerations (200–1000 deg/s² versus 8–260 deg/s² in human studies). Consistent with this
566 interpretation, at the lowest acceleration tested, roll latencies approached values previously
567 reported in humans, reinforcing the role of acceleration in determining response onset.

568 It is noteworthy that previous work in patients with proprioceptive deficits (Carpenter et al.,
569 2001) and vestibular loss (Horak et al., 2016), as well as studies using galvanic vestibular
570 stimulation (Horak & Hlavacka, 2002), suggests that short-latency responses are dominated by
571 proprioceptive inputs, with vestibular contributions emerging at longer latencies. For
572 translational perturbations, otolith afferents encode linear acceleration (or jerk under highly
573 dynamic conditions; Jamali et al., 2013, 2019), limiting velocity-dependent effects. In contrast,
574 during rotational perturbations, semicircular canals encode angular velocity—and acceleration
575 under dynamic conditions (Jamali et al., 2016; Sadeghi et al., 2007), allowing both kinematic
576 variables to shape postural responses. Nevertheless, across perturbation types, platform motion
577 ultimately induces whole-body sway, requiring continuous monitoring of body motion relative to
578 gravity and the support surface (Mergner et al., 2009; Peterka, 2018). The conserved sequence
579 of acceleration- and velocity-modulated response phases observed here, corresponding to
580 previously reported EMG bursts (Diener et al., 1983; Dunbar et al., 1986), supports a general
581 control mechanism regulating postural dynamics across axes.

582 *Rhesus macaques as a platform for circuit-level dissection of balance control*

583 Rhesus macaques provide a valuable translational bridge between classical animal models and
584 human studies of postural control. While cats have traditionally served as models for postural
585 reflexes, macaques share over 97% genomic similarity with humans (Gibbs et al., 2007), exhibit
586 similar head-movement statistics during natural behaviors (Carriot et al., 2017), and—unlike
587 digitigrade cats—are plantigrade, bearing weight across the entire foot. This posture imposes
588 biomechanical demands for standing balance that closely resemble those in humans.
589 Consistent with this alignment, rhesus monkey CoP responses—particularly in roll—closely
590 parallel those reported in humans (Dunbar et al., 1986), despite earlier response onsets
591 consistent with body scaling, indicating conserved neural control strategies across primates. In
592 contrast, differences in body plan shape responses to pitch perturbations, whereas roll
593 responses remain highly similar across species. Together, these findings establish behavioral
594 benchmarks for interpreting postural control in the macaque model. Because this model permits
595 invasive recordings and causal circuit manipulations not feasible in humans, future studies can
596 determine how neural population activity contributes to distinct temporal phases of the postural
597 response and evaluate potential vestibular prosthetic interventions (Boutros et al., 2019;
598 Wiboonsaksakul et al., 2022, 2023).

599 Our experiments focused on transient perturbations, leaving open whether acceleration- and
600 velocity-dependent control generalizes to prolonged or stochastic disturbances encountered
601 during natural behavior. Moreover, although our approach isolates the kinematic variables
602 shaping postural responses, the sensory–motor circuits implementing these axis-dependent
603 strategies remain unknown. Future studies combining this perturbation framework with neural
604 recordings or causal manipulations in rhesus monkeys will be essential for linking circuit
605 dynamics to the temporal phases of balance control and guiding vestibular prosthetic strategies.

606

607 **Acknowledgements**

608 We would like to thank the entire Cullen Lab especially Dale Roberts, Walter Kucharski, and
609 Balazs Vagvolgyi for their technical support; and Pum Wiboonsaksakul, Robyn Mildren, Lex
610 Gómez, Skyler Thomas, Chenhao Bao, and Oliver Stanley for their advice and comments on
611 the manuscript and figures. We would also like to thank the animal care and veterinary staff as
612 well as our animal subjects. This research was supported by grants R01DC002390 &
613 R01DC018061 from the National Institutes of Health (K.E.C.), as well as Ruth L. Kirchstein
614 National Research Service Award F31DC020390 (O.L.B.).

615 **Author Contributions**

616 **O.M.E.L.B.:** Conceptualization, Methodology, Software, Formal Analysis, Investigation, Data
617 Curation, Visualization, Writing – Original Draft, Writing – Review & Editing. **B.A.R.:**
618 Investigation, Data Curation, Writing – Review & Editing. **K.E.C.:** Conceptualization, Resources,
619 Writing – Review & Editing, Supervision, Funding Acquisition.

620 **Conflict of Interest**

621 The authors have no competing financial interests to declare.

622 **Data Availability**

623 Data and analysis code are available from the corresponding author upon reasonable request.

624

625 **References**

- 626 Allum, J. H. J. (1992). *A postural model of balance-correcting movement strategies*. Journal of
627 Vestibular Research. <https://pubmed.ncbi.nlm.nih.gov/1342406/>
- 628 Allum, J. H. J., Honegger, F., & Schicks, H. (1994). The influence of a bilateral peripheral
629 vestibular deficit on postural synergies - PubMed. *Journal of Vestibular Research*, 4(1), 49–
630 70. <https://pubmed.ncbi.nlm.nih.gov/8186863/>
- 631 Allum, J. H. J., Carpenter, M. G., & Honegger, F. (2003). Directional Aspects of Balance
632 Corrections in Man. *IEEE Engineering in Medicine and Biology Magazine*, 22(2), 37–47.
633 <https://doi.org/10.1109/MEMB.2003.1195694>
- 634 Allum, J. H. J., Oude Nijhuis, L. B., & Carpenter, M. G. (2008). Differences in coding provided by
635 proprioceptive and vestibular sensory signals may contribute to lateral instability in
636 vestibular loss subjects. *Exp Brain Res*, 184, 391–410. <https://doi.org/10.1007/s00221-007-1112-z>
- 638 Allum, J. H. J., & Pfaltz, C. R. (1985). Visual and vestibular contributions to pitch sway
639 stabilization in the ankle muscles of normals and patients with bilateral peripheral vestibular
640 deficits. *Experimental Brain Research*, 58(1), 82–94. <https://doi.org/10.1007/BF00238956>
- 641 Bloem, B., Allum, J. H. J., Carpenter, M., Verschuuren, J., & Honegger, F. (2002). Triggering of
642 balance corrections and compensatory strategies in a patient with total leg proprioceptive
643 loss. *Experimental Brain Research*, 142(1), 91–107. <https://doi.org/10.1007/s00221-001-0926-3>
- 645 Boutros, P. J., Valentin, N. S., Hageman, K. N., Dai, C., Roberts, D., & Della Santina, C. C.
646 (2019). Nonhuman primate vestibuloocular reflex responses to prosthetic vestibular
647 stimulation are robust to pulse timing errors caused by temporal discretization. *Journal of*
648 *Neurophysiology*, 121(6), 2256–2266. <https://doi.org/10.1152/jn.00887.2018>
- 649 Buchanan, J. J., & Horak, F. B. (2001). Emergence of postural patterns as a function of vision
650 and translation frequency. *Journal of Neurophysiology*, 85(5), 1988–2000.
651 <https://doi.org/10.1152/jn.2001.85.5.1988>
- 652 Carpenter, M., Allum, J. H. J., & Honegger, F. (2001). Vestibular influences on human postural
653 control in combinations of pitch and roll planes reveal differences in spatiotemporal
654 processing. *Experimental Brain Research* 2001 140:1, 140(1), 95–111.
655 <https://doi.org/10.1007/S002210100802>
- 656 Carriot, J., Jamali, M., Chacron, M. J., & Cullen, K. E. (2017). The statistics of the vestibular
657 input experienced during natural self-motion differ between rodents and primates. *The*
658 *Journal of Physiology*, 595(8), 2751. <https://doi.org/10.1113/JP273734>
- 659 Cullen, K. E. (2019). Vestibular processing during natural self-motion: implications for
660 perception and action. *Nature Reviews Neuroscience*, 20, 346–363.
661 <https://doi.org/10.1038/s41583-019-0153-1>
- 662 Diener, H. C., Bootz, F., Dichgans, J., & Bruzek, W. (1983). Variability of postural 'reflexes' in
663 humans. *Experimental Brain Research*, 52(3), 423–428.
664 <https://doi.org/10.1007/BF00238035>

- 665 Diener, H. C., Horak, F. B., & Nashner, L. M. (1988). Influence of Stimulus Parameters on
666 Human Postural Responses. *Journal of Neurophysiology*, 59(6), 1888–1905.
667 www.physiology.org/journal/jn
- 668 Dunbar, D. C., Horak, F. B., Macpherson, J. M., & Rushmer, D. S. (1986). Neural control of
669 quadrupedal and bipedal stance: Implications for the evolution of erect posture. *American*
670 *Journal of Physical Anthropology*, 69(1), 93–105.
671 <https://doi.org/10.1002/AJPA.1330690111>
- 672 Forbes, P. A., Chen, A., & Blouin, J. S. (2018). Sensorimotor control of standing balance.
673 *Handbook of Clinical Neurology*, 159, 61–83. [https://doi.org/10.1016/B978-0-444-63916-](https://doi.org/10.1016/B978-0-444-63916-5.00004-5)
674 [5.00004-5](https://doi.org/10.1016/B978-0-444-63916-5.00004-5)
- 675 Forbes, P. A., Kwan, A., Rasman, B. G., Mitchell, D. E., Cullen, K. E., & Blouin, J.-S. (2020).
676 Neural mechanisms underlying high frequency vestibulocollic reflexes in humans and
677 monkeys. *Journal of Neuroscience*.
- 678 Fryar, C. D., Carroll, M. D., Gu, Q., Afful, J., & Ogden, C. L. (2021). Anthropometric Reference
679 Data for Children and Adults: United States, 2015-2018 - PubMed. *Vital Health Statistics*,
680 3(36), 1–44. <https://pubmed.ncbi.nlm.nih.gov/33541517/>
- 681 Gibbs, R. A., Rogers, J., Katze, M. G., Bumgarner, R., Weinstock, G. M., Mardis, E. R.,
682 Remington, K. A., Strausberg, R. L., Venter, J. C., Wilson, R. K., Batzer, M. A.,
683 Bustamante, C. D., Eichler, E. E., Hahn, M. W., Hardison, R. C., Makova, K. D., Miller, W.,
684 Milosavljevic, A., Palermo, R. E., ... Zwiag, A. S. (2007). Evolutionary and Biomedical
685 Insights from the Rhesus Macaque Genome. *Science*, 316(5822), 222–234.
686 <https://doi.org/10.1126/SCIENCE.1139247>
- 687 Goldberg, J., & Peterson, B. W. (1986). Reflex and mechanical contributions to head
688 stabilization in alert cats. <https://doi.org/10.1152/Jn.1986.56.3.857>, 56(3), 857–875.
689 <https://doi.org/10.1152/JN.1986.56.3.857>
- 690 Goodworth, A., Felmlee, D., & Karmali, F. (2023). Variation between individuals in sensorimotor
691 feedback control of standing balance. *Journal of Neurophysiology*, 130(2), 303–318.
692 <https://doi.org/10.1152/JN.00353.2022>
- 693 Horak, F. B., & Hlavacka, F. (2002). Vestibular and somatosensory contributions to responses
694 to head and body displacements in stance. *Experimental Brain Research*, 144(4), 460–
695 468. <https://doi.org/10.1007/s00221-002-1037-4>
- 696 Horak, F. B., Kluzik, J., & Hlavacka, F. (2016). Velocity dependence of vestibular information for
697 postural control on tilting surfaces. <https://doi.org/10.1152/Jn.00057.2016>, 116(3), 1468–
698 1479. <https://doi.org/10.1152/JN.00057.2016>
- 699 Horak, F. B., & Macpherson, J. M. (1996). Postural Orientation and Equilibrium. *Comprehensive*
700 *Physiology*, 255–292. <https://doi.org/10.1002/CPHY.CP120107>
- 701 Horak, F. B., Nashner, L. M., & Diener, H. C. (1990). Postural strategies associated with
702 somatosensory and vestibular loss. *Experimental Brain Research*, 82(1), 167–177.
703 <https://doi.org/10.1007/BF00230848>

704 Inglis, J. T., & Macpherson, J. M. (1995). Bilateral labyrinthectomy in the cat: effects on the
705 postural response to translation. <https://doi.org/10.1152/Jn.1995.73.3.1181>, 73(3), 1181–
706 1191. <https://doi.org/10.1152/JN.1995.73.3.1181>

707 Jacobs, R., & Macpherson, J. M. (1996). Two functional muscle groupings during postural
708 equilibrium tasks in standing cats. *Journal of Neurophysiology*, 76(4), 2402–2411.
709 <https://doi.org/10.1152/JN.1996.76.4.2402>

710 Jamali, M., Carriot, J., Chacron, M. J., & Cullen, K. E. (2013). Strong correlations between
711 sensitivity and variability give rise to constant discrimination thresholds across the otolith
712 afferent population. *Journal of Neuroscience*, 33(27), 11302–11313.
713 <https://doi.org/10.1523/JNEUROSCI.0459-13.2013>

714 Jamali, M., Carriot, J., Chacron, M. J., & Cullen, K. E. (2019). Coding strategies in the otolith
715 system differ for translational head motion vs. static orientation relative to gravity. *Elife*, 8,
716 e45573.

717 Jamali, M., Chacron, M. J., & Cullen, K. E. (2016). Self-motion evokes precise spike timing in
718 the primate vestibular system. *Nature Communications*, 7.
719 <https://doi.org/10.1038/NCOMMS13229>

720 Kakara, R. S., Lee, R., & Eckstrom, E. N. (2024). Cause-Specific Mortality Among Adults Aged
721 ≥65 Years in the United States, 1999 Through 2020. *Public Health Reports*, 139(1), 54–58.
722 <https://doi.org/10.1177/00333549231155869>

723 Karashchuk, P., Rupp, K. L., Dickinson, E. S., Walling-Bell, S., Sanders, E., Azim, E., Brunton,
724 B. W., & Tuthill, J. C. (2021). Anipose: A toolkit for robust markerless 3D pose estimation.
725 *Cell Reports*, 36(13), 109730. <https://doi.org/10.1016/j.celrep.2021.109730>

726 Keshner, E. A., Baker, J. F., Banovetz, J., & Peterson, B. W. (1992). Patterns of neck muscle
727 activation in cats during reflex and voluntary head movements. *Experimental Brain*
728 *Research* 1992 88:2, 88(2), 361–374. <https://doi.org/10.1007/BF02259112>

729 Keshner, E. A., & Dhaher, Y. (2008). Characterizing head motion in three planes during
730 combined visual and base of support disturbances in healthy and visually sensitive
731 subjects. *Gait and Posture*, 28(1), 127–134. <https://doi.org/10.1016/j.gaitpost.2007.11.003>

732 Kong, P. W., Beauchamp, G., Suyama, J., & Hostler, D. (2010). Effect of fatigue and
733 hypohydration on gait characteristics during treadmill exercise in the heat while wearing
734 firefighter thermal protective clothing. *Gait & Posture*, 31(2), 284–288.
735 <https://doi.org/10.1016/J.GAITPOST.2009.11.006>

736 Küng, U. M., Horlings, C. G. C., Honegger, F., Duysens, J. E. J., & Allum, J. H. J. (2009).
737 Control of roll and pitch motion during multi-directional balance perturbations. *Experimental*
738 *Brain Research*, 194(4), 631–645. <https://doi.org/10.1007/S00221-009-1743-3/FIGURES/9>

739 Lemay, J. F., Gagnon, D., Nadeau, S., Grangeon, M., Gauthier, C., & Bherer, L. (2014). Center-
740 of-pressure total trajectory length is a complementary measure to maximum excursion to
741 better differentiate multidirectional standing limits of stability between individuals with
742 incomplete spinal cord injury and able-bodied individuals. *Journal of NeuroEngineering and*
743 *Rehabilitation*, 11, 8. <https://doi.org/10.1186/1743-0003-11-8>

- 744 Lippi, V., Maurer, C., & Mergner, T. (2023). Human body-sway steady-state responses to small
745 amplitude tilts and translations of the support surface – Effects of superposition of the two
746 stimuli. *Gait & Posture*, *100*, 139–148. <https://doi.org/10.1016/J.GAITPOST.2022.12.003>
- 747 Macpherson, J. M., Everaert, D. G., Stapley, P. J., & Ting, L. H. (2007). Bilateral Vestibular Loss
748 in Cats Leads to Active Destabilization of Balance During Pitch and Roll Rotations of the
749 Support Surface. *J. Neurophysiol*, *97*, 4357–4367. <https://doi.org/10.1152/jn.01338.2006>
- 750 Maki, B. E., & Ostrovski, G. (1993). Do postural responses to transient and continuous
751 perturbations show similar vision and amplitude dependence? *Journal of Biomechanics*,
752 *26*(10), 1181–1190. [https://doi.org/10.1016/0021-9290\(93\)90066-N](https://doi.org/10.1016/0021-9290(93)90066-N)
- 753 Mansfield, A., & Maki, B. E. (2009). Are age-related impairments in change-in-support balance
754 reactions dependent on the method of balance perturbation? *Journal of Biomechanics*,
755 *42*(8), 1023–1031. <https://doi.org/10.1016/J.JBIOMECH.2009.02.007>
- 756 Mathis, A., Mamidanna, P., Cury, K. M., Abe, T., Murthy, V. N., Mathis, M. W., & Bethge, M.
757 (2018). DeepLabCut: markerless pose estimation of user-defined body parts with deep
758 learning. *Nature Neuroscience*, *21*(9), 1281–1289. <https://doi.org/10.1038/S41593-018-0209-Y;SUBJMETA>
- 760 Mergner, T. (2007). Modeling sensorimotor control of human upright stance. *Progress in Brain*
761 *Research*, *165*, 283–297. [https://doi.org/10.1016/S0079-6123\(06\)65018-8](https://doi.org/10.1016/S0079-6123(06)65018-8)
- 762 Mergner, T., Schweigart, G., & Fennell, L. (2009). Vestibular humanoid postural control. *Journal*
763 *of Physiology-Paris*, *103*(3–5), 178–194.
764 <https://doi.org/10.1016/J.JPHYSPARIS.2009.08.002>
- 765 Missen, K. J., Asslander, L., Babichuk, A., Chua, R., Inglis, J. T., & Carpenter, M. G. (2023).
766 The role of torque feedback in standing balance. *Journal of Neurophysiology*, *130*(3), 585–
767 595. <https://doi.org/10.1152/JN.00046.2023>
- 768 Moreland, B., Kakara, R., & Henry, A. (2023). Trends in Nonfatal Falls and Fall-Related Injuries
769 Among Adults Aged ≥65 Years — United States, 2012–2018. *Morbidity and Mortality*
770 *Weekly Report*, *69*(27), 875–881. <https://doi.org/10.15585/MMWR.MM6927A5>
- 771 Peng, G. C. Y., Hain, T. C., & Peterson, B. W. (1996). A dynamical model for reflex activated
772 head movements in the horizontal plane. *Biological Cybernetics*, *75*(4), 309–319.
773 <https://doi.org/10.1007/S004220050297/METRICS>
- 774 Peterka, R. J. (2002). Sensorimotor integration in human postural control. *J Neurophysiol*, *88*,
775 1097–1118. <https://doi.org/10.1152/jn.00605.2001>
- 776 Peterka, R. J. (2018). Sensory integration for human balance control. In *Handbook of Clinical*
777 *Neurology* (Vol. 159, pp. 27–42). Elsevier B.V. <https://doi.org/10.1016/B978-0-444-63916-5.00002-1>
- 778
- 779 Sadeghi, S. G., Chacron, M. J., Taylor, M. C., & Cullen, K. E. (2007). Neural variability,
780 detection thresholds, and information transmission in the vestibular system. *Journal of*
781 *Neuroscience*, *27*(4), 771–781. <https://doi.org/10.1523/JNEUROSCI.4690-06.2007>

- 782 Thompson, L. A., Haburcakova, C., & Lewis, R. F. (2016). Vestibular ablation and a semicircular
783 canal prosthesis affect postural stability during head turns. *Experimental Brain Research*,
784 234(11), 3245–3257. <https://doi.org/10.1007/s00221-016-4722-5>
- 785 Ting, L. H., & Macpherson, J. M. (2004). Ratio of Shear to Load Ground-Reaction Force May
786 Underlie the Directional Tuning of the Automatic Postural Response to Rotation and
787 Translation. <https://doi.org/10.1152/Jn.00773.2003>, 92(2), 808–823.
788 <https://doi.org/10.1152/JN.00773.2003>
- 789 Torres-Oviedo, G., Macpherson, J. M., & Ting, L. H. (2006). Muscle synergy organization is
790 robust across a variety of postural perturbations. *Journal of Neurophysiology*, 96(3), 1530–
791 1546. <https://doi.org/10.1152/jn.00810.2005>
- 792 Vagvolgyi, B. P., Jayakumar, R. P., Madhav, M. S., Knierim, J. J., & Cowan, N. J. (2022). Wide-
793 angle, monocular head tracking using passive markers. *Journal of Neuroscience Methods*,
794 368, 109453. <https://doi.org/10.1016/J.JNEUMETH.2021.109453>
- 795 Vilensky, J. A. (1979). Masses, centers-of-gravity, and moments-of-inertia of the body segments
796 of the rhesus monkey (*Macaca mulatta*). *American Journal of Physical Anthropology*, 50(1),
797 57–65. <https://doi.org/10.1002/AJPA.1330500109>
- 798 Welch, T. D. J., & Ting, L. H. (2009). A Feedback Model Explains the Differential Scaling of
799 Human Postural Responses to Perturbation Acceleration and Velocity. *Journal of*
800 *Neurophysiology*, 101(6), 3294. <https://doi.org/10.1152/JN.90775.2008>
- 801 Wiboonsaksakul, K. P., Della Santina, C. C., & Cullen, K. E. (2023). Prosthetic Stimulation of
802 the Vestibular Nerve Can Evoke Robust Eye and Head Movements Despite Prior
803 Labyrinthectomy. *Otology & Neurotology: Official Publication of the American Otological*
804 *Society, American Neurotology Society [and] European Academy of Otology and*
805 *Neurotology*. <https://doi.org/10.1097/MAO.0000000000004007>
- 806 Wiboonsaksakul, K. P., Roberts, D. C., Santina, C. C. D., & Cullen, K. E. (2022). A prosthesis
807 utilizing natural vestibular encoding strategies improves sensorimotor performance in
808 monkeys. *PLOS Biology*, 20(9), e3001798.
809 <https://doi.org/10.1371/JOURNAL.PBIO.3001798>
- 810 Zobeiri, O. A., & Cullen, K. E. (2022). Distinct Representations of Body and Head motion are
811 Dynamically Encoded by Purkinje cell Populations in the Macaque Cerebellum. *ELife*, 11.
812 <https://doi.org/10.7554/ELIFE.75018>

813

814 Figure Legends

815 **Figure 1.** Experimental paradigm and conceptual framework. (A) Rhesus monkeys stood freely
816 on a force plate mounted to a hexapod motion platform while head kinematics were measured
817 using an inertial measurement unit (IMU). Center-of-pressure (CoP) was computed from
818 ground-reaction forces recorded beneath each limb. (B) Transient rotational perturbations were
819 applied in pitch (forward/backward) and roll (left/right). (C) Perturbation profiles were designed
820 to independently vary peak velocity while holding angular acceleration constant (top), or vary
821 angular acceleration while holding peak velocity constant (bottom). (D) A simple dual-pendulum
822 model (see Methods) illustrating how variation in body–platform coupling and neck stiffness can
823 produce distinct head and body kinematics, providing a conceptual framework for distinguishing
824 platform-following behavior from active stabilization.

825 **Figure 2.** Postural responses to forward pitch perturbations of varying peak velocity in the axis
826 of the perturbation. (A) Head pitch velocity, head fore-aft acceleration, and fore-aft CoP
827 responses of “Monkey D” to perturbations with peak velocities of 20 (purple), 40 (blue), and 60
828 (green) deg/s and acceleration of 500 deg/s². Traces show the mean response over 20 trials
829 and shaded regions represent the mean +/- SEM. (B) Quantified head pitch velocity response.
830 Dots and open circles represent individual trials, pooled across monkeys. Filled circles indicate
831 statistical significance (ANOVA $p < 0.025$) for comparison across velocities accounting for
832 differences between individual monkeys. Open circles indicate lack of statistical significance
833 (ANOVA $p > 0.025$). Bold black lines indicate a linear velocity-dependent trend (regression
834 $p < 0.05$). From left to right: Yellow region: mean head pitch velocity in the short-latency window
835 (ANOVA $p = 0.59$). Green region: mean head pitch velocity in the medium-latency window
836 (ANOVA $p = 0.000943$, regression $p = 0.000543$). White background, left: response onset latency
837 (ANOVA $p = 0.35$). White background, right: total head pitch displacement (ANOVA $p = 0.050372$).
838 Dotted black line indicates perfect riding response, solid black line indicates perfect
839 compensatory response leading to no head-in-space motion. See Figure S1 for mean
840 responses of individual monkeys. (C) Quantified head fore-aft acceleration response, same
841 format as (B). From left to right, mean acceleration in the short-latency window (ANOVA
842 $p = 0.61$), mean acceleration in the medium-latency window (ANOVA $p = 0.000615$, regression
843 $p = 6.26e-5$), response onset latency (ANOVA $p = 0.53$), and linear displacement (ANOVA
844 $p = 0.68227$). (D) Quantified CoP fore-aft response, same format as (B) and (C) From left to right,
845 mean CoP response in the short-latency window (ANOVA $p = 0.0016$, regression $p = 0.000572$),
846 mean CoP response in the medium-latency window (ANOVA $p = 0.0202$, regression $p = 0.0163$),
847 CoP response onset latency (ANOVA $p = 0.96$), and CoP distance traversed (ANOVA $p = 0.0350$).

848 **Figure 3.** Postural responses to backward pitch perturbations of varying peak velocity in the
849 axis of the perturbation. (A) Head pitch velocity, head fore-aft acceleration, and fore-aft CoP
850 responses of “Monkey D” to perturbations with peak velocities of 20 (purple), 40 (blue), and 60
851 (green) deg/s and acceleration of 500 deg/s². Traces show the mean response over 20 trials
852 and shaded regions represent the mean +/- SEM. (B) Quantified head pitch velocity response,
853 same plotting conventions as Figure 2. From left to right: Yellow region: mean head pitch
854 velocity in the short-latency window (ANOVA $p = 0.64$). Green region: mean head pitch velocity in
855 the medium-latency window (ANOVA $p = 0.000218$, regression $p = 8.70e-5$). White background,
856 left: response onset latency (ANOVA $p = 0.45$). White background, right: total head pitch
857 displacement (ANOVA $p = 0.00319$, regression $p = 0.0203$). Dotted black line indicates perfect
858 riding response, solid black line indicates perfect compensatory response leading to no head-in-

859 space motion. See Figure S2 for mean responses of individual monkeys. (C) Quantified head
860 fore-aft acceleration response, same format as (B). From left to right, mean acceleration in the
861 short-latency window (ANOVA $p=0.41$), mean acceleration in the medium-latency window
862 (ANOVA $p=2.24e-5$, regression $p=0.00344$), response onset latency (ANOVA $p=0.92$) linear
863 displacement (ANOVA $p=0.23$). (D) Quantified CoP fore-aft response, same format as (B) and
864 (C) From left to right, mean CoP response in the short-latency window (ANOVA $p=0.000189$,
865 regression $p=1.77e-5$), mean CoP response in the medium-latency window (ANOVA
866 $p=0.00386$, regression $p=0.00369$), CoP response onset latency (ANOVA $p=0.84$) CoP distance
867 traversed (ANOVA $p=0.86$).

868 **Figure 4.** Postural responses to roll perturbations of varying peak velocity in the axis of the
869 perturbation. (A) Head roll velocity, head lateral acceleration, and lateral CoP responses of
870 “Monkey D” to perturbations with peak velocities of 20 (red), 40 (orange), and 60 (yellow) deg/s
871 and acceleration of 500 deg/s². Traces show the mean response over 20 trials and shaded
872 regions represent the mean +/- SEM. (B) Quantified head roll velocity response, same plotting
873 conventions as Figure 2. From left to right: Yellow region: mean head roll velocity in the short-
874 latency window (ANOVA $p=0.0104$). Green region: mean head roll velocity in the medium-
875 latency window (ANOVA $p=0.0210$, regression $p=0.00883$). White background, left: response
876 onset latency (ANOVA $p=0.59$). White background, right: total head roll displacement (ANOVA
877 $p=0.79$). Dotted black line indicates perfect riding response, solid black line indicates perfect
878 compensatory response leading to no head-in-space motion. See Figure S4 for mean
879 responses of individual monkeys. (C) Quantified head lateral acceleration response, same
880 format as (B). From left to right, mean acceleration in the short-latency window (ANOVA
881 $p=0.60$), mean acceleration in the medium-latency window (ANOVA $p=0.00195$, regression
882 $p=0.00107$), response onset latency (ANOVA $p=0.47$) linear displacement (ANOVA $p=0.76$). (D)
883 Quantified CoP lateral response, same format as (B) and (C) From left to right, mean CoP
884 response in the short-latency window (ANOVA $p=1.81e-11$, regression $p=2.54e-11$), mean CoP
885 response in the medium-latency window (ANOVA $p=0.000533$, regression $p=0.000608$), CoP
886 response onset latency (ANOVA $p=0.39$) CoP distance traversed (ANOVA $p=0.0448$).

887 **Figure 5.** Postural responses to forward pitch perturbations of varying acceleration in the axis of
888 the perturbation. (A) Head pitch velocity, head fore-aft acceleration, and fore-aft CoP responses
889 of “Monkey D” to perturbations with accelerations of 200 (purple), 500 (blue), and 1000 (green)
890 deg/s² and velocity of 40 deg/s. Traces show the mean response over 20 trials and shaded
891 regions represent the mean +/- SEM. (B) Quantified head pitch velocity response. Dots and
892 open circles represent individual trials, pooled across monkeys. Filled circles indicate statistical
893 significance (ANOVA $p<0.025$) for comparison across velocities accounting for differences
894 between individual monkeys. Open circles indicate lack of statistical significance (ANOVA
895 $p>0.025$). Bold black lines indicate a linear acceleration-dependent trend (regression $p<0.05$).
896 From left to right: Yellow region: mean head pitch velocity in the short-latency window (ANOVA
897 $p=0.0218$, regression $p=0.0384$). Green region: mean head pitch velocity in the medium-latency
898 window (ANOVA $p=0.00204$, regression $p=0.33$). White background, left: response onset
899 latency (ANOVA $p=0.17$). White background, right: total head pitch displacement (ANOVA
900 $p=0.35$). Dotted black line indicates perfect riding response, solid black line indicates perfect
901 compensatory response leading to no head-in-space motion. See Figure S5 for mean
902 responses of individual monkeys. (C) Quantified head fore-aft acceleration response, same
903 format as (B). From left to right, mean acceleration in the short-latency window (ANOVA
904 $p=0.47$), mean acceleration in the medium-latency window (ANOVA $p=0.096$), response onset

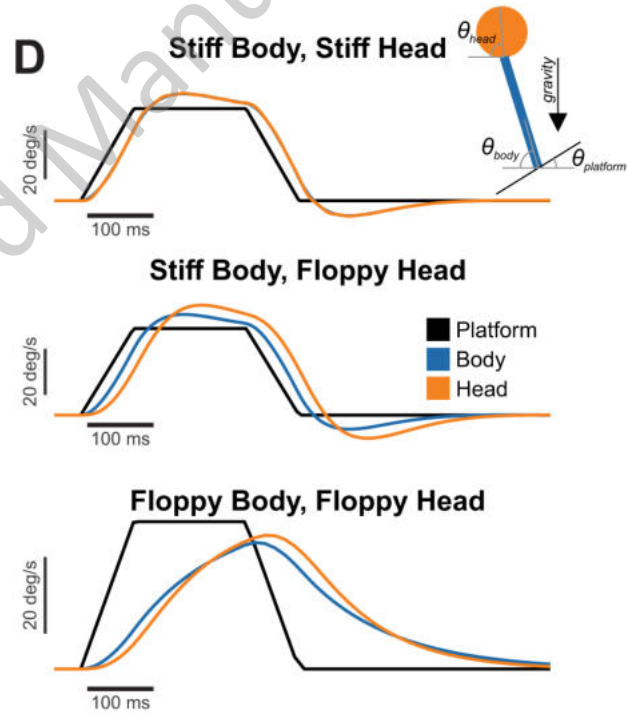
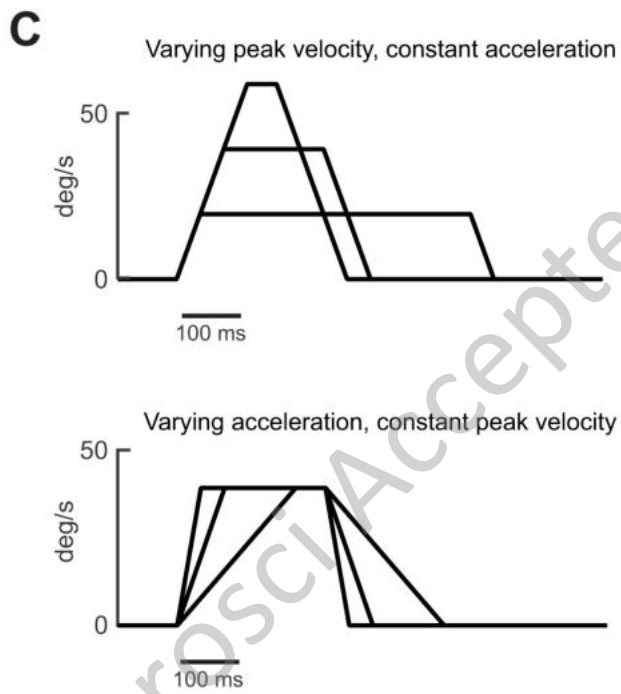
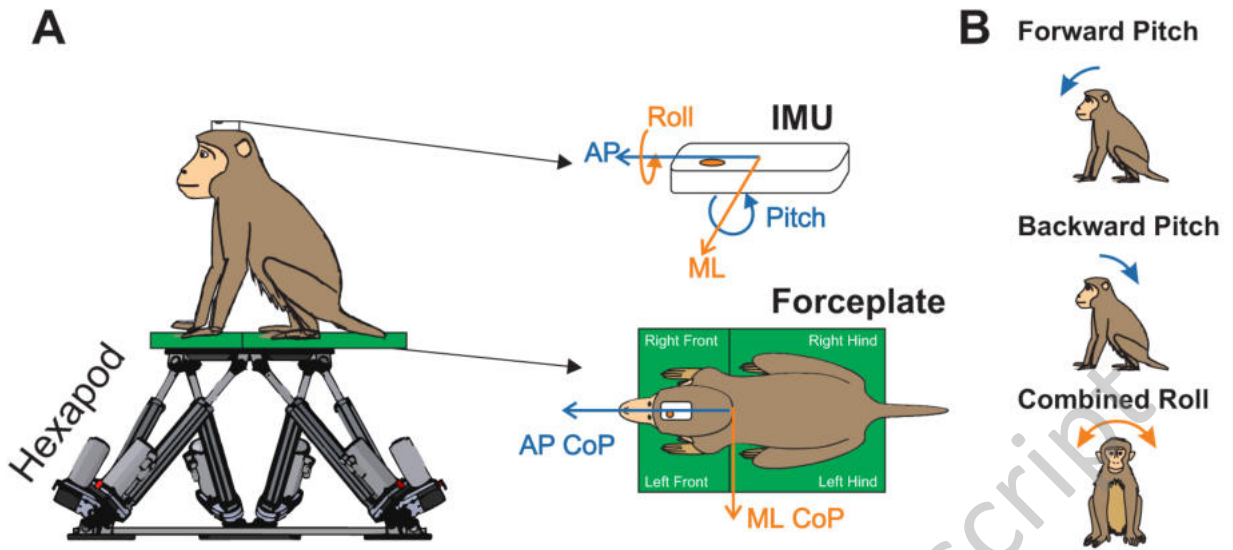
905 latency (ANOVA $p=0.45$) linear displacement (ANOVA $p=0.25$). (D) Quantified CoP fore-aft
906 response, same format as (B) and (C). From left to right, mean CoP response in the short-
907 latency window (ANOVA $p=2.46e-6$, regression $p=1.23e-5$), mean CoP response in the
908 medium-latency window (ANOVA $p=0.28$), CoP response onset latency (ANOVA $p=0.00103$,
909 regression $p=0.00307$), and CoP distance traversed (ANOVA $p=0.34$).

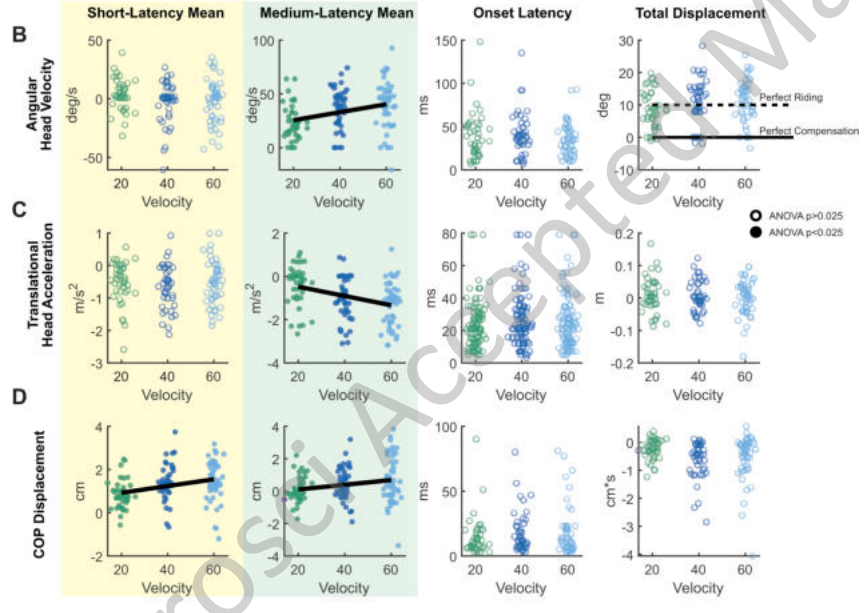
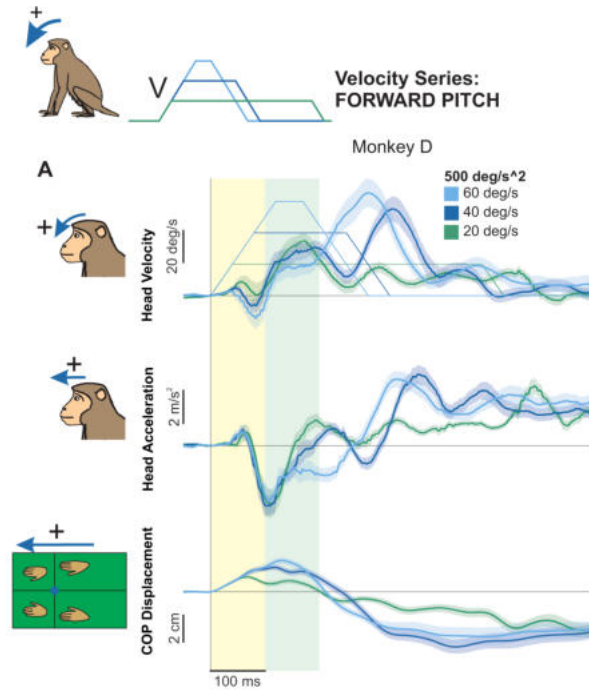
910 **Figure 6.** Postural responses to backward pitch perturbations of varying acceleration in the axis
911 of the perturbation. (A) Head pitch velocity, head fore-aft acceleration, and fore-aft CoP
912 responses of “Monkey D” to perturbations with accelerations of 200 (purple), 500 (blue), and
913 1000 (green) deg/s^2 and velocity of 40 deg/s . Traces show the mean response over 20 trials
914 and shaded regions represent the mean \pm SEM. (B) Quantified head pitch velocity response,
915 same plotting conventions as Figure 5. From left to right: Yellow region: mean head pitch
916 velocity in the short-latency window (ANOVA $p=0.72$). Green region: mean head pitch velocity in
917 the medium-latency window (ANOVA $p=0.34$). White background, left: response onset latency
918 (ANOVA $p=0.000172$, regression $p=0.000157$). White background, right: total head pitch
919 displacement (ANOVA $p=0.0184$, regression $p=0.63$). Dotted black line indicates perfect riding
920 response, solid black line indicates perfect compensatory response leading to no head-in-space
921 motion. See Figure S6 for mean responses of individual monkeys. (C) Quantified head fore-aft
922 acceleration response, same format as (B). From left to right, mean acceleration in the short-
923 latency window (ANOVA $p=0.00266$, regression $p=0.00115$), mean acceleration in the medium-
924 latency window (ANOVA $p=0.00101$, regression $p=0.000209$), response onset latency (ANOVA
925 $p=0.68$) linear displacement (ANOVA $p=0.65$). (D) Quantified CoP fore-aft response, same
926 format as (B) and (C) From left to right, mean CoP response in the short-latency window
927 (ANOVA $p=0.000540$, regression $p=0.000700$), mean CoP response in the medium-latency
928 window (ANOVA $p=0.18$), CoP response onset latency (ANOVA $p=0.000753$, regression
929 $p=0.00167$), and CoP distance traversed (ANOVA $p=0.78$).

930 **Figure 7.** Postural responses to roll perturbations of varying acceleration in the axis of the
931 perturbation. (A) Head roll velocity, head lateral acceleration, and lateral CoP responses of
932 “Monkey D” to perturbations with accelerations of 200 (red), 500 (orange), and 1000 (yellow)
933 deg/s^2 and velocity of 40 deg/s . Traces show the mean response over 20 trials and shaded
934 regions represent the mean \pm SEM. (B) Quantified head roll velocity response. Dots and open
935 circles represent individual trials, pooled across monkeys, same plotting conventions as Figure
936 5. From left to right: Yellow region: mean head roll velocity in the short-latency window (ANOVA
937 $p=0.29$). Green region: mean head roll velocity in the medium-latency window (ANOVA
938 $p=0.00383$, regression $p=0.00337$). White background, left: response onset latency (ANOVA
939 $p=0.0112$, regression $p=0.0362$). White background, right: total head roll displacement (ANOVA
940 $p=0.45$). Dotted black line indicates perfect riding response, solid black line indicates perfect
941 compensatory response leading to no head-in-space motion. See Figure S7 for mean
942 responses of individual monkeys. (C) Quantified head lateral acceleration response, same
943 format as (B). From left to right, mean acceleration in the short-latency window (ANOVA
944 $p=0.00903$, regression $p=0.00487$), mean acceleration in the medium-latency window (ANOVA
945 $p=0.30$), response onset latency (ANOVA $p=0.049$), and linear displacement (ANOVA $p=0.27$).
946 (D) Quantified CoP lateral response, same format as (B) and (C) From left to right, mean CoP
947 response in the short-latency window (ANOVA $p=1.55e-14$, regression $p=6.05e-10$), mean CoP
948 response in the medium-latency window (ANOVA $p=0.549$), CoP response onset latency
949 (ANOVA $p=9.472e-6$, regression $p=0.000218$) CoP distance traversed (ANOVA $p=0.56$).

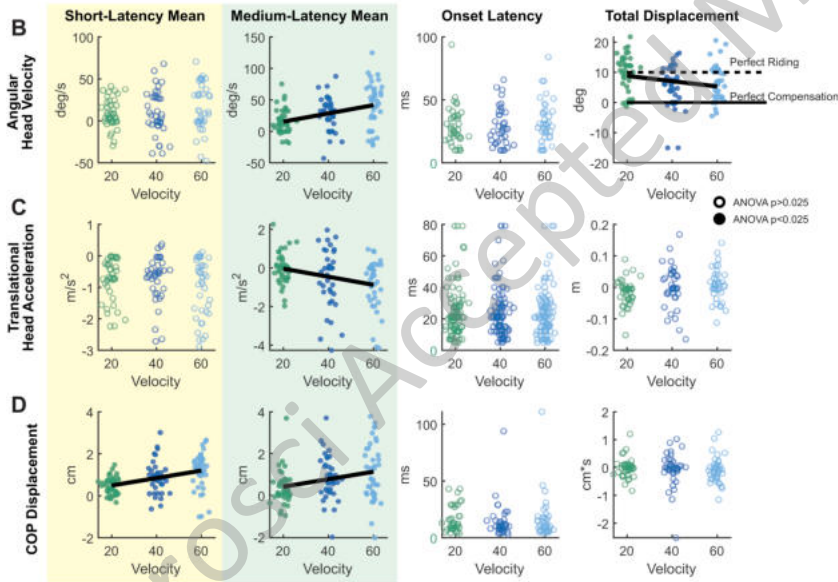
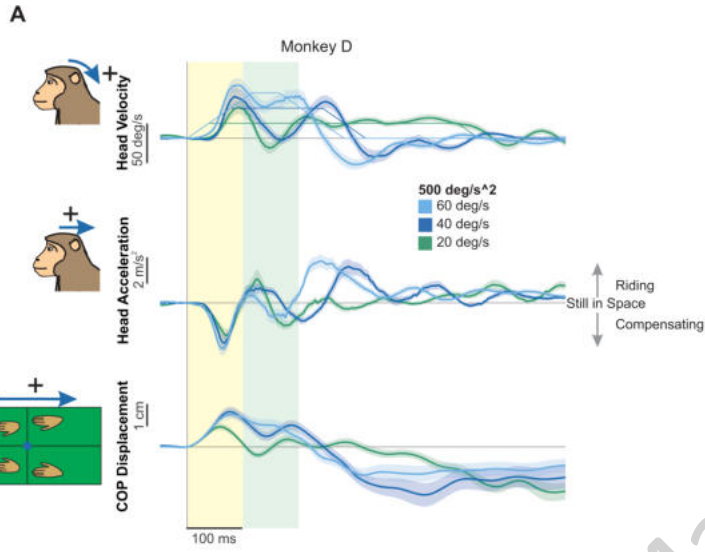
950 **Figure 8.** Dissociation of postural strategies across pitch and roll axes. (A) Total head angular
951 displacement for pitch perturbations (left) and roll perturbations (right), pooled across all velocity
952 and acceleration conditions. Individual trials are shown as dots. Dashed black line: theoretical
953 "perfect riding" response (head displacement = platform displacement = 10°). Solid black line:
954 theoretical "perfect compensation" (head displacement = 0° , indicating complete stabilization in
955 space). Pitch displacements clustered at or above 10° , consistent with a passive platform-
956 following strategy. Roll displacements fell between 0° and 10° , indicating partial active
957 compensation. (B) Representative video frames from single trials illustrating postural strategy.
958 Pitch (left): the body remains aligned with the tilting platform, consistent with platform-following.
959 Roll (right): the body remains closer to vertical despite platform tilt, consistent with stabilization
960 relative to space.

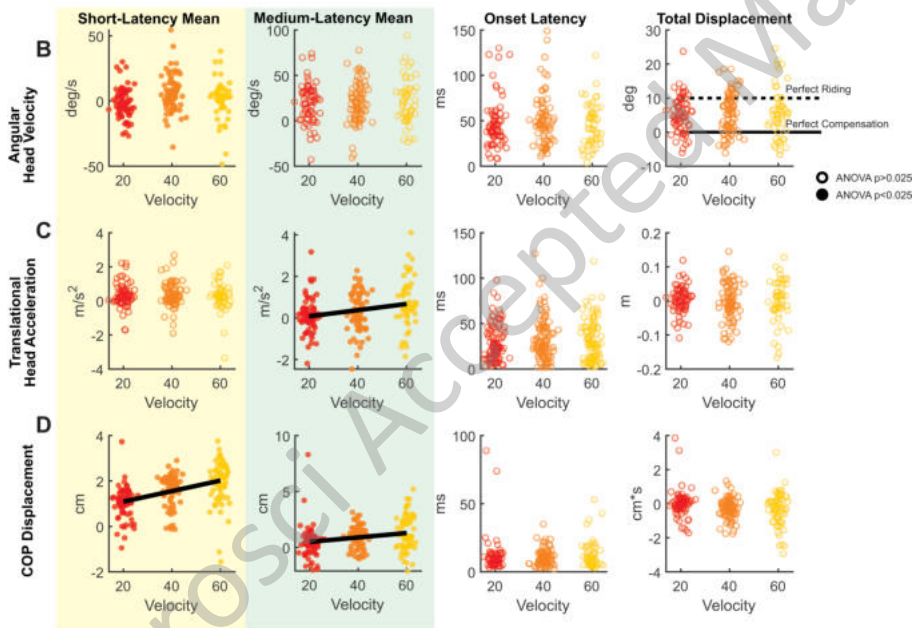
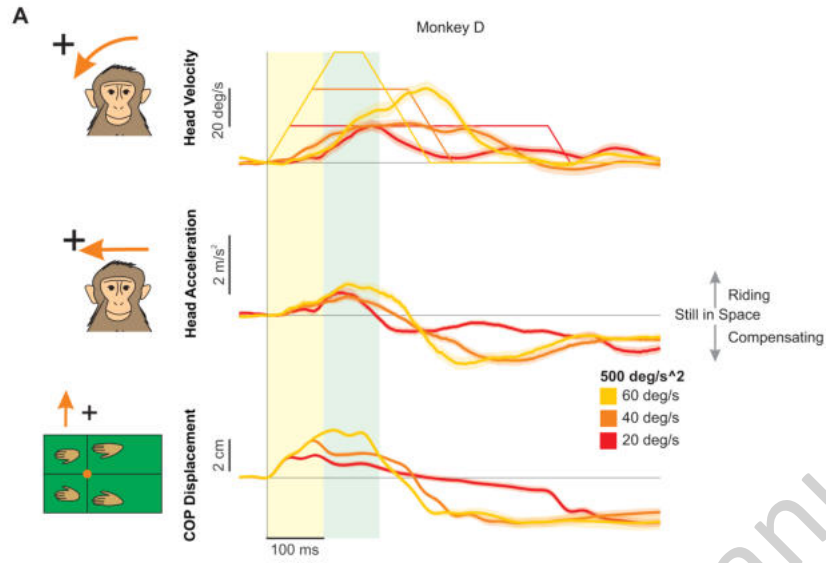
JNeurosci Accepted Manuscript



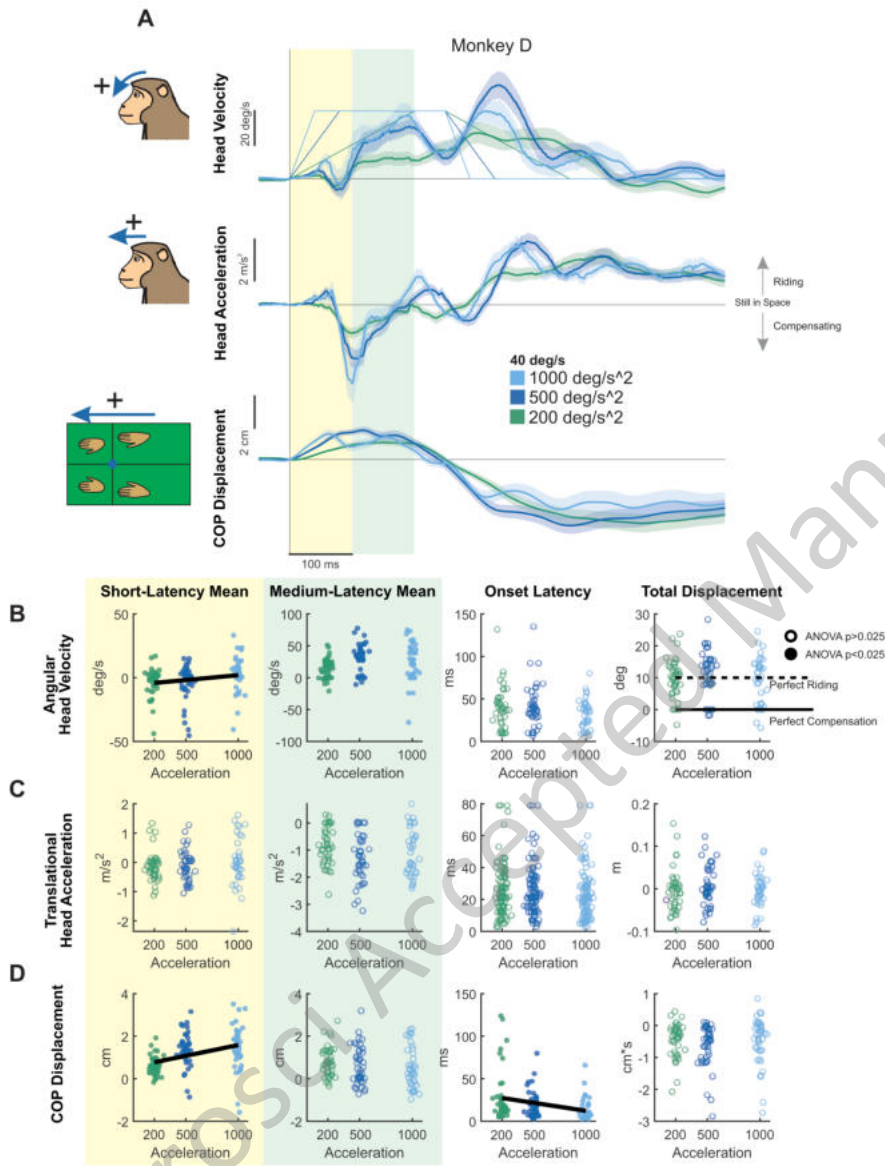


JNeurosci Accepted Manuscript

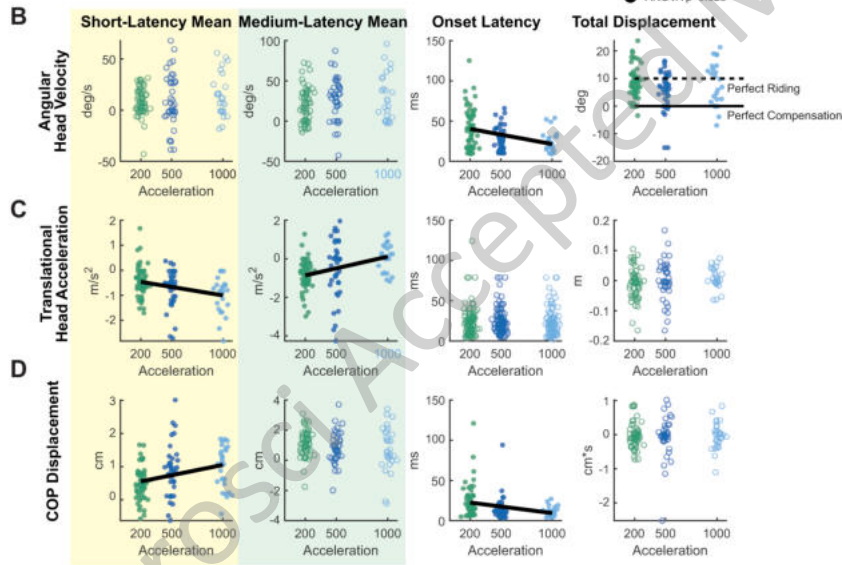
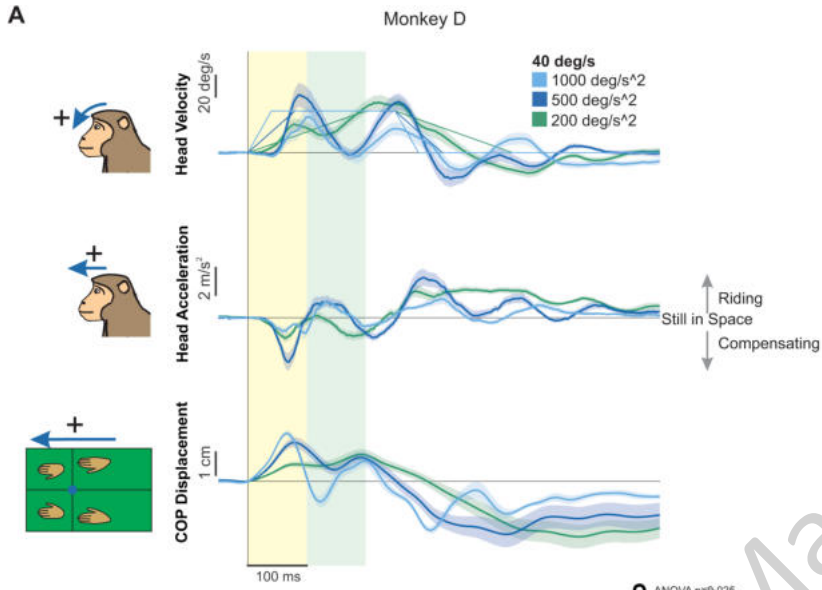


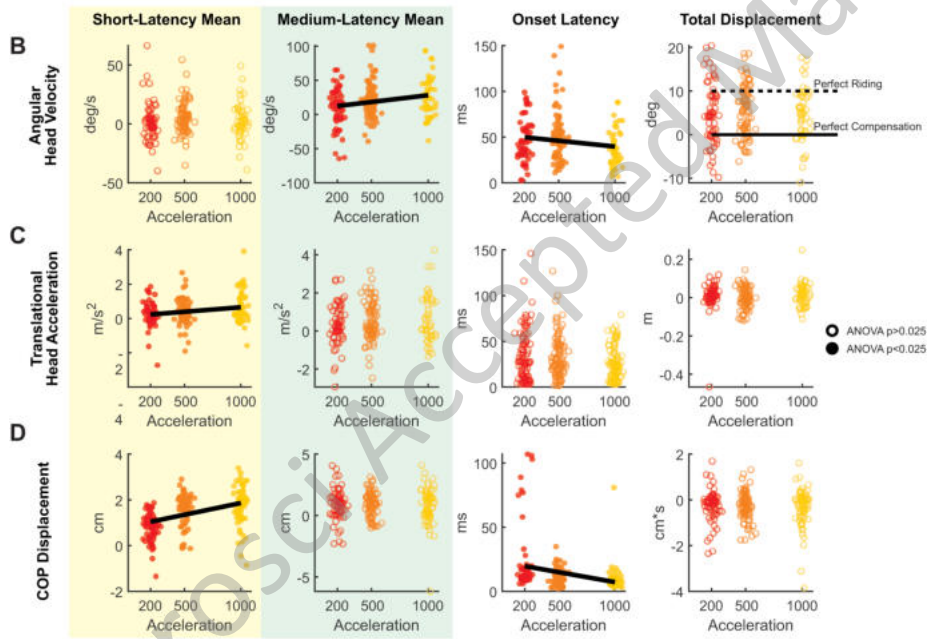
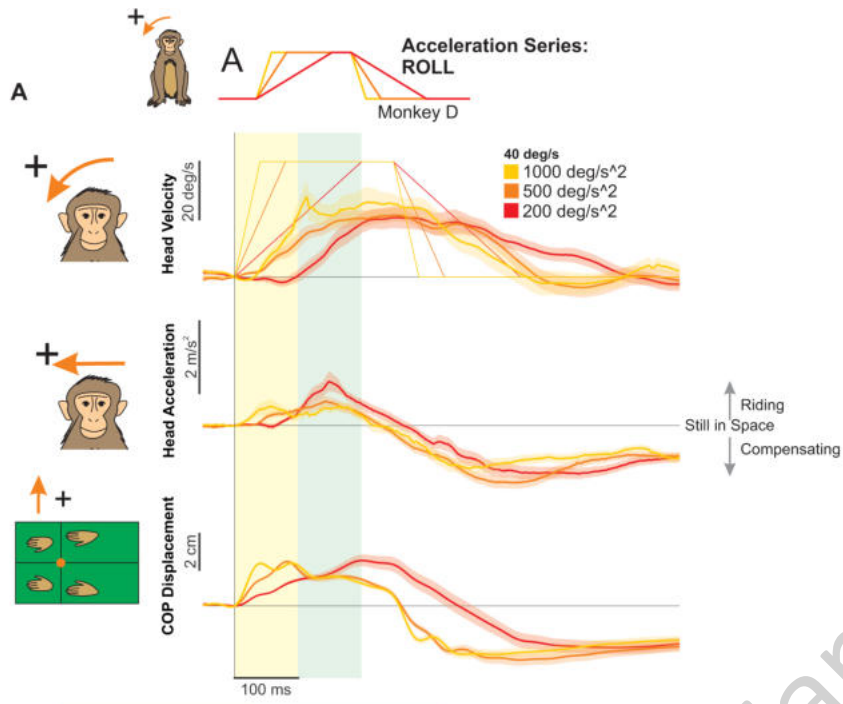


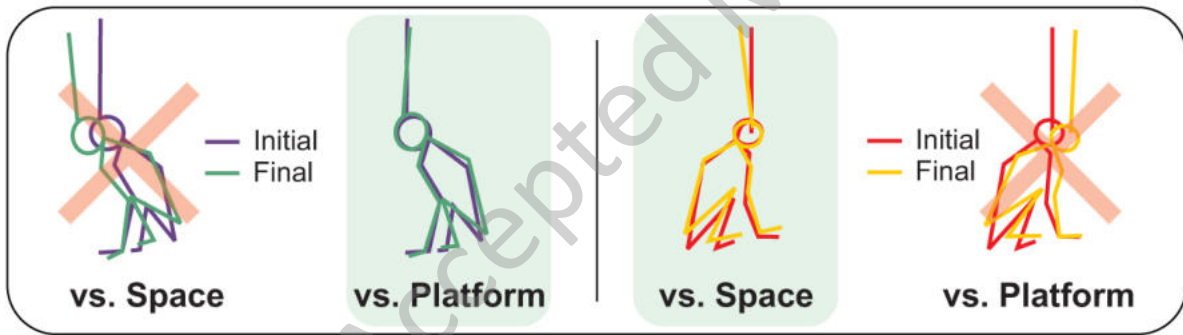
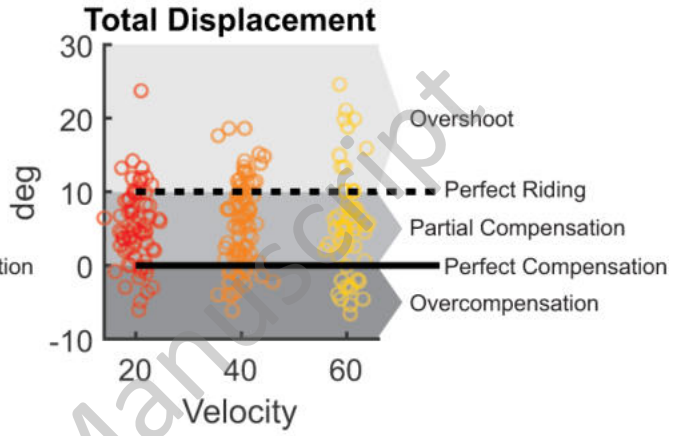
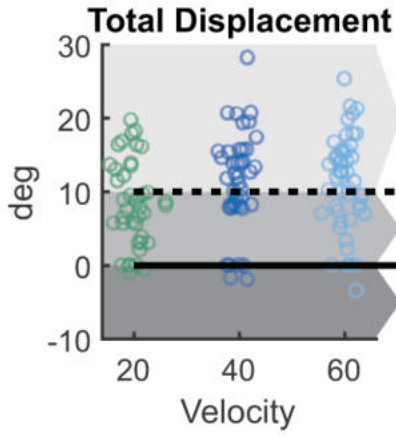
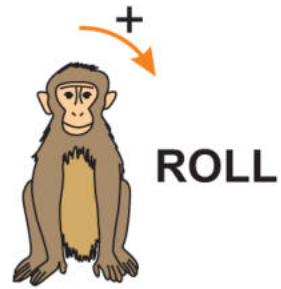
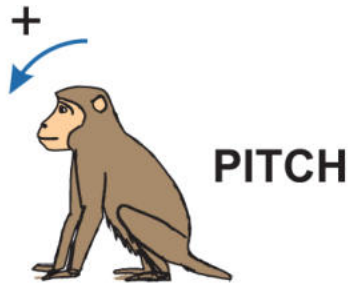
Acceleration Series: FORWARD PITCH



Accepted Manuscript







JNeurosci Accepted Manuscript